Vol. 25, No. 1(2026) Ener26700

Revista Mexicana de Ingeniería Química

A geochemical diagnostic tool for enhanced oil recovery in a Low Salinity Waterflooding process in carbonates

Una herramienta de diagnóstico geoquímico para la recuperación mejorada de aceite en un proceso de Inyección de Agua de Baja Salinidad en carbonatos

J.M. Carmona-Pérez[1]*, M.A. Díaz-Viera[1], E. Serrano-Saldaña[1], B. Carreón-Calderón[1], M. Coronado[1], M.P Andersson[2]

[1]*Instituto Mexicano del Petróleo, Eje Central Lázaro Cárdenas, 07730, Ciudad de México, México.*

[2]*King Fahd University of Petroleum and Minerals, Academic Belt Road, 31261, Dhahran, Saudi Arabia.*

Received: October 29, 2025; Accepted: December 18, 2025

Abstract

Laboratory-scale brine design to optimize oil recovery in low-salinity waterflood processes is expensive, largely unrepresentative, and time-consuming. This study aimed to develop a fast diagnostic tool by extending the theoretical Bond Product Sum (BPS) mechanism for decision-making on the feasibility of this enhanced oil recovery (EOR) process. An integrated methodology was formulated that combines geochemical equilibrium calculations to estimate BPS values with pore network modeling to predict oil recovery. The tool was validated using spontaneous imbibition experiments performed on Bedford limestone cores with seven brine compositions. The results demonstrated a consistent inverse relationship between BPS and oil recovery.

In particular, BPS values decreased from 1.805×10^{-9} mol/m^2 for formation water to 1.753×10^{-9} mol/m^2 for seawater, correlating with a 27% reduction in residual oil saturation. This suggests that the electrostatic attraction at the interface is weakened with optimized brines, leading to improved recoveries. We conclude that this BPS-based diagnostic tool offers a more efficient and reliable alternative to traditional experiments for designing optimal brine compositions in carbonate reservoirs.

Keywords: Low Salinity Waterflooding, Geochemical Modeling, Bond Product Sum, Carbonate Reservoirs, Enhanced Oil Recovery, Pore Network Modeling.

Resumen

El diseño de salmueras a escala de laboratorio para optimizar la recuperación de petróleo en procesos de inyección de agua de baja salinidad es costoso, poco representativo y consume mucho tiempo. Este estudio tuvo como objetivo desarrollar una herramienta de diagnóstico rápida extendiendo el mecanismo teórico de la Suma del Producto de Enlaces (BPS, por sus siglas en inglés) para la toma de decisiones sobre la viabilidad de este proceso de recuperación mejorada de petróleo (EOR). Se formuló una metodología integrada que combina cálculos de equilibrio geoquímico para estimar los valores de BPS con modelado de redes de poros para predecir la recuperación de petróleo. La herramienta fue validada mediante experimentos de imbibición espontánea realizados en núcleos de caliza de Bedford con siete composiciones de salmuera. Los resultados demostraron una relación inversa consistente entre el BPS y la recuperación de petróleo.

En particular, los valores de BPS disminuyeron de $1,805 \times 10^{-9}$ para el agua de formación a $1,753 \times 10^{-9}$ mol/m^2 para el agua de mar, lo que se correlaciona con una reducción del 27% en la saturación de petróleo residual. Esto sugiere que la atracción electrostática en la interfaz se debilita con las salmueras optimizadas, lo que conduce a mejores recuperaciones. Concluimos que esta herramienta de diagnóstico basada en BPS ofrece una alternativa más eficiente y confiable a los experimentos tradicionales para diseñar composiciones de salmuera óptimas en yacimientos de carbonatos.

Palabras clave: Inyección de Agua de Baja Salinidad, Modelado Geoquímico, Suma del Producto de Enlaces, Yacimientos de Carbonatos, Recuperación Mejorada de Petróleo, Modelado de Redes de Poros.

* *Corresponding author. E-mail*: carmona.jesus.94@gmail.com ;

https://doi.org/10.24275/rmiq/Ener26700

ISSN:1665-2738, *issn-e*: 2395-8472

1 Introduction

Geochemical reactions at the crude oil-brine-rock (COBR) interface are important interactions that influence oil recovery (Alghamdi *et al.,* 2017; Brady, Krumhansl, and Mariner 2012; Brady and Krumhansl 2013). Understanding the relationship between molecular and macroscopic oil recovery is important to bridge the gap from molecular level surface complexation mechanisms to field scale enhanced oil recovery applications.

Carbonate reservoirs are predominantly mixed-wet to oil-wet state due to the adsorption of polar oil components onto mineral surfaces through electrostatic bonding between carboxylic acid groups (-COOH) and calcium sites ($>CaOH_2^+$), nitrogen base groups ($-NH_4^+$) with carbonate sites ($>CO_3^-$), and divalent cation bridging where Ca^{2+} and Mg^{2+} ions bond negatively charged carboxylates to negatively charged mineral surfaces (Brady and Thyne 2016; Buckley *et al.,* 1998; Lager *et al.,* 2006).

One promising enhanced oil recovery method that has gained considerable attention is Low Salinity Waterflooding (LSWF) due to its ability to disrupt the surface complexation reactions at the COBR interface, thereby reducing electrostatic bond strengths between oil and mineral surfaces and promoting wettability alteration toward more water-wet state (Almasiyan and Mahani 2024; Austad *et al.,* 2012; Brady, Krumhansl, and Mariner 2012; Mahani, Keya, and Berg 2015; Zhang *et al.,* 2007).

In the LSWF state-of-the-art, researchers have investigated several mechanisms responsible for oil recovery. The pH effect has been extensively studied, with findings demonstrating that in the pH range 5.5-6.5, reducing brine salinity leads to a decrease in contact angle, thus indicating a shift towards a water-wet state (Mahani, Menezes, *et al.,* 2017; Xie, Sari, *et al.,* 2018).

Temperature influence represents another significant mechanism, with studies revealing that higher temperatures effectively promote interactions between multivalent Mg^{2+}, SO_4^{2-} and Ca^{2+} ions (Gachuz-Muro 2013; Mahani, Menezes, *et al.,* 2017; Tetteh, Brady, and Ghahfarokhi 2021; Xie, Brady, *et al.,* 2017). Multicomponent ionic exchange has also been observed, where SO_4^{2-} ions adsorb onto positively charged water-wet sites, causing a reduction in electrostatic allowing more Ca^{2+} to adhere to the mineral surface and form bonds with $-COO^-$ groups (Dang 2013; Kwak *et al.,* 2014; Omekeh *et al.,* 2012).

Research on interfacial tension has consistently shown that LSWF can significantly reduce the interfacial tension, which facilitates oil recovery (Alvarado *et al.,* 2014; Deng *et al.,* 2021; Derkani *et al.,* 2018; Lashkarbolooki *et al.,* 2014; Rahevar *et al.,* 2023; Wei *et al.,* 2017). Additionally, wettability alteration studies have demonstrated that LSWF disrupts the equilibrium at the oil-rock interface, causing a transition from oil-wet or mixed-wet conditions to a more favorable water-wet state, especially when multivalent ions like Mg^{2+}, SO_4^{2-}, and Ca^{2+} are present in the brine composition (Chandrasekhar and Mohanty 2013; Korrani *et al.,* 2015; Zhang *et al.,* 2007).

Mineral dissolution has also been identified as another mechanism, where the increased negative charge on carbonate surfaces resulting from dissolution actively promotes interactions between Ca^{2+} ions and carboxylic functional groups (Morse *et al.,* 2002; Ouden 2014; Qiao, Li, *et al.,* 2015; Qiao, Johns, and Li 2016). Despite this extensive research, there remains considerable controversy surrounding which mechanism contributes most to the effectiveness of LSWF in enhancing oil recovery.

As far as experimental methods are concerned, most work has focused on laboratory scale studies including coreflooding experiments (Gachuz-Muro and Sohrabi 2017; Reinoso *et al.,* 2024; Yousef *et al.,* 2011) and spontaneous imbibition tests (Gachuz-Muro and Sohrabi 2014; Reinoso *et al.,* 2024; Yu *et al.,* 2009; Zaeri *et al.,* 2018; Zhang *et al.,* 2007) to investigate optimal brine compositions for the LSWF process. Other EOR techniques, such as emulsion flooding, have also demonstrated effectiveness in improving sweep efficiency through pore blocking mechanisms in sandstone reservoirs (Olivares-Xometl *et al.,* 2024). One of the major drawbacks of using any of these laboratory scale experiments is the time consumption and financial resource requirements. Despite these limitations, there remains a critical need for an efficient diagnostic tool capable of simulating various brine compositions while accounting for geochemical reactions at the COBR interface. Such a tool would rapidly predict the most optimal brine formulation for oil recovery without the time and resource constraints of traditional laboratory methodology.

One quantitative mechanism that addresses the geochemical reactions at the oil-rock interface is the bond product sum (BPS), which provides a molecular-level understanding of wettability alterations. Brady and Thyne (2016) introduced BPS as a measure of electrostatic attractions between oppositely charged species at oil-rock interface, establishing geochemical reactions for predicting wettability changes. Erzuah *et al.,* (2017) validated the BPS approach through surface complexation modeling coupled with flotation experiments for quartz, kaolinite, and calcite minerals, demonstrating strong agreement between predicted electrostatic pair linkages and experimental wettability measurements. Subsequently, Chen *et al.,* (2018), Tetteh, Brady, and Ghahfarokhi

(2021) and Almasiyan and Mahani (2024) further demonstrated that BPS calculations could accurately predict wettability trends with varying salinity and pH conditions by analyzing specific surface sites such as $>CaOH_2^+$, $>CaSO_4^-$, $>CaCO_3^-$, $>CO_3^-$, $>CO_3Ca^+$, and $>CO_3Mg^+$.

Although BPS has shown theoretical promise in understanding geochemical interactions at the COBR interface, the direct application to practical oil recovery scenarios does not exist. Additionally, there is no methodology for applying BPS mechanism to rapidly screen and optimize brine composition.

The present study aims to extend the BPS theoretical findings of Brady and Thyne (2016), Erzuah *et al.,* (2017), Chen *et al.,* (2018), Tetteh, Brady, and Ghahfarokhi (2021), Almasiyan and Mahani (2024) to practical applications by analyzing how different brine compositions affect wettability and oil recovery in spontaneous imbibition experiments using Bedford limestone samples. Our step-by-step methodology, which serves as a diagnostic tool, introduces a rapid assessment of how various brine compositions influence wettability alterations.

Additionally, to model oil recovery performance, we adopted an approach that incorporated three complementary techniques in order to simulate and predict spontaneous imbibition recovery factors. First, we used pore network modeling using OpenPNM software (Gostick, Aghighi, Hinebaugh, Tranter, Hoeh, Day, Spellacy, Sharqawy, Bazylak, Burns, and Lehnert 2016) to simulate fluid displacement behavior at the pore scale through invasion percolation algorithms, which enabled us to model the fundamental physics of oil recovery processes. Subsequently, we applied a modified Brooks-Corey model to establish empirical relationships between computed brine saturation data and relative permeability functions, allowing us to quantify fluid flow characteristics essential for oil recovery modeling. Finally, we used McWhorter and Sunada (1990) analytical solutions to predict spontaneous imbibition recovery factors based on material balance principles, which provided us with direct quantitative predictions of oil recovery performance.

The structure of the paper is as follows: section 2 presents the experimental results of spontaneous imbibition in four limestone core samples from Bedford. Section 3 describes the geochemical methodology developed. In the sections 4, 5 and 6 are presented the spontaneous imbibition tests, contact and interfacial tension, and BPS and ionic strength results, respectively. In section 7 presents the methodology validation in a case study. Finally, the conclusions are given in section 8.

2 Materials and experimental setup

In the present study, we utilize the results from core sample Ls2 as a case to validate the proposed concept of bond product sum. Detailed experimental information for all samples (Ls2, Ls3, Ls5, and Ls6) is organized in the following subsections, covering brine composition, petrophysical properties, oil characteristics, and experimental procedures.

2.1 Bedford core sample

Four limestone core samples (Ls2, Ls3, Ls5, and Ls6) taken from the Salem formation located in South Indiana, USA, also known as Bedford limestone, were used in a spontaneous imbibition experiment. The cores were prepared following the standard procedure described by the Laboratory of the Mexican Petroleum Institute (Serrano-Saldaña 2018). The aim of this procedure was to ensure consistent initial conditions and restore reservoir wettability.

Our procedure consisted of the following steps. The core samples were first fully saturated with distilled water. This allows for the calculation of the pore volume (PV) and porosity. After full water saturation, the cores were brought to initial fluid saturation conditions. In standard core analysis, this refers to displacing the mobile water with oil to create a representative initial water saturation (Swi) and initial oil saturation (Soi) that mimic reservoir conditions. This is typically done by injecting and flooding the core with oil. The cores, now at Swi/Soi, were then aged in the crude oil for two weeks. This is a critical step to restore the wettability of the rock surface to a more representative reservoir condition by allowing adsorption of polar components from the crude oil. The aging procedure was conducted at a constant temperature of 65°C. After aging, the excess oil was removed, and the sample was weighted. The volumes of oil (Soi) and water (Swi) inside the core were then known and could be reported as a percentage of the pore volume.

Figure 1 shows a representative example of the core samples used in this study, displaying the Bedford limestone sample Ls2 from multiple perspectives.

Table 1 details the characteristics of the four Bedford limestone cores (Ls2, Ls3, Ls5, and Ls6) selected for this analysis. The samples have lengths ranging from 6.86 to 6.92 cm and diameters from 3.50 to 3.71 cm. They demonstrate porosity values between 14.8% and 15.6% and pore volumes of 10.1 to 11.6 mL. Our measurements showed absolute water permeability varied from 16.8 to 33.3 mD. Under irreducible water saturation (S_{wirr}) conditions, water occupied 35.3% to 49.7% of the pore volume, while

the remaining 50.3% to 64.7% contained the non-wetting phase.

Fig. 1: Photographic images of Bedford limestone core Ls2 used in the spontaneous imbibition tests.

Table 1. Petrophysical characteristics of Bedford limestone core samples used in spontaneous imbibition experiments

Sample ID	Length (cm)	Diameter (cm)	Porosity (%)	Pore Volume (mL)	Absolute Permeability (mD)	S_{wirr} (% PV)	Initial Oil Saturation (% PV)
Ls2	6.92	3.50	15.2	10.1	16.8	35.3	64.7
Ls3	6.86	3.61	14.8	10.4	33.3	48.7	51.3
Ls5	6.89	3.65	14.9	10.8	25.2	45.9	54.1
Ls6	6.87	3.71	15.6	11.6	28.5	49.7	50.3

Table 2. Characterization of the crude oil.

Property	Value
API gravity (°)	30.3
Density at 70 °C (g/cm³)	0.84
Viscosity at 90 °C (cP)	2.24
TAN (mg KOH/g)	0.03
TBN (mg KOH/g)	1.92
Sulfur content (wt%)	1.63
SARA Composition (wt%)	
Saturates	56.27
Aromatics	34.85
Resins	7.98
Asphaltenes	0.9

2.2 *Oil sample characterization*

The crude oil used in this study was a dead oil sample obtained from an oil field in southern Mexico. An analyses of the crude oil was calculated, with the properties detailed in Table 2.

The oil was characterized as a light crude oil with an API gravity of 30.3°. Additional measurements revealed a total acid number (TAN) of 0.09 mg KOH/g and a total base number (TBN) of 0.24 mg KOH/g. SARA (Saturates, Aromatics, Resins, and Asphaltenes) analysis was conducted, showing a composition of 56.27% saturates, 34.85% aromatics, 7.98% resins, and 0.9% asphaltenes. It should be noted that asphaltene content varies significantly among crude oils, ranging from less than 1% to over 20% depending on the geological origin and maturity of the petroleum system (Serrano-Saldaña 2018). The relatively low asphaltene content of this particular sample is characteristic of light crude oils from this specific geological formation in southern Mexico.

2.3 *Brine composition design*

A series of brine compositions was designed to investigate the effects of ionic composition and salinity on spontaneous imbibition. The brines used in this study, as shown in Table 3, consisted of formation water (FW) the connate water trapped in the reservoir pore spaces and a synthetic formulation representing the seawater (SW) along with their respective dilutions and specific ionic modifications. The seawater compositions SW6 and SW7 correspond to a reference seawater composition and its half-diluted version, respectively.

Table 3. Brine compositions used in spontaneous imbibition experiments

	FW (mol/L)	**FW/2** (mol/L)	**FW/2 + $MgSO_4$** (mol/L)	**FW/4** (mol/L)	**FW/4 + $MgSO_4$** (mol/L)	**SW6** (mol/L)	**SW7** (mol/L)
Na^+	1.81	0.91	0.91	0.45	0.45	0.47	0.23
Cl^-	3.24	1.62	1.62	0.81	0.81	0.54	0.27
Ca^{2+}	0.65	0.32	0.32	0.16	0.16	0.01	0.05
Mg^{2+}	0.07	0.03	0.05	0.02	0.03	0.05	0.03
SO_4^{2-}	0.00	0.00	0.02	0.00	0.02	0.03	0.01
TDS (g/L)	**184.09**	**92.03**	**94.03**	**46.05**	**48.05**	**34.45**	**17.23**

Table 4. Spontaneous Imbibition Test Sequences for Individual Core Samples

Sample ID	**First Brine**	**Second Brine**	**Third Brine**	**Fourth Brine**
Ls2	FW	FW/2	FW/2 + $MgSO_4$	SW6
Ls3	FW/2	FW/2 + $MgSO_4$	FW/4	SW7
Ls5	FW/2 + $MgSO_4$	FW/4	FW/4 + $MgSO_4$	SW7
Ls6	FW/4	FW/4 + $MgSO_4$	SW6	SW7

Note: All spontaneous imbibition tests were conducted at a constant temperature of 65°C.

Following the stiff diagrams reported by Serrano-Saldaña 2018 for a brine sample from a southern Mexico oil field reservoir, formation water was synthetically formulated with a pH of 6. To systematically evaluate the impact of decreasing salinity, dilution factors FW/2, SW6 and FW/4, SW7 were applied. Furthermore, specific compositions were modified by the addition of potential determining ions, such as Mg^{2+} and SO_4^{2-}, to investigate their contribution to wettability alteration.

The specific brine order applied to each individual Bedford limestone sample during the spontaneous imbibition tests are presented in Table 4. This approach was designed to analyze the evaluation of both salinity effects and the contribution of potential determining ions in enhancing oil recovery.

2.4 Spontaneous imbibition test setup

Spontaneous imbibition is a phenomenon by which one fluid displaces another in a porous medium, utilizing only capillary forces. This process plays a significant role in the secondary recovery of hydrocarbons, particularly in fractured reservoirs where the oil is absorbed by large blocks of rock surrounded by fractures. However, it is important to note that in fractured porous medium, multiple mechanisms including gravitational drainage, block size distribution, and flow velocity become increasingly relevant, making imbibition one of several contributing factors rather than the sole recovery mechanism.

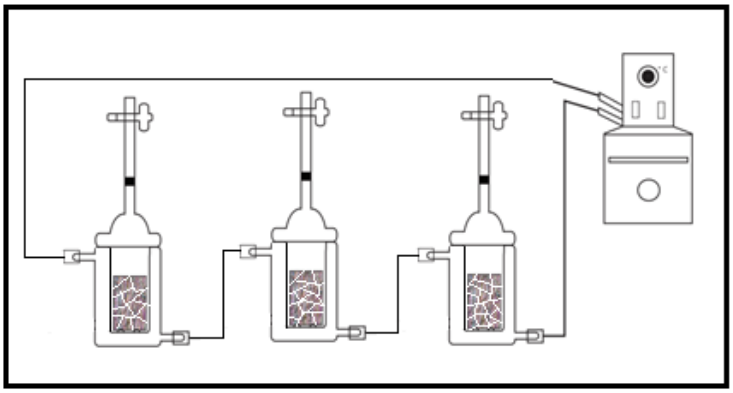

Fig. 2: Diagram of the imbibition equipment in Amott cell.

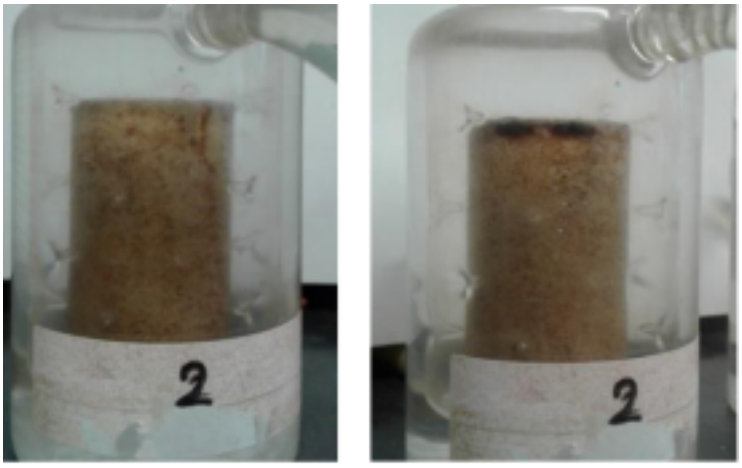

Fig. 3: Ls2 sample undergoing imbibition with FW brine. The left side represents the initial setup at Day 0, while the right side after 15 days of imbibition at 65°C.

Figure 2 shows the experimental setup used to carry out the spontaneous imbibition test, which consists of an Amott cell, temperature bath, and digital camera system.

The experimental procedure was conducted as follows. Initially, each core sample, previously saturated with water under irreducible conditions and aged in dead oil, was removed and excess oil was carefully removed. The prepared sample was then placed in the Amott cell and flooded with the first imbibition brine in the sequence. During the initial stage, samples underwent spontaneous imbibition for a period of 15 days at a constant temperature of 65°C. The recovery process was monitored through systematic photographic documentation to track temporal oil recovery behavior, as shown in Figure 3 which shows the Ls2 sample during imbibition with FW brine. At each stage, the imbibition fluid was drained and the total volume of recovered oil was measured. Subsequently, each sample was subjected to the next brine composition in the predetermined sequence, with this procedure repeated systematically for all subsequent stages.

2.5 *Contact angle and interfacial tension estimation procedure*

2.5.1 *Contact angle measurement*

The wettability of the rock-fluid system was evaluated through contact angle measurements using the pendant drop method. These measurements were performed following a high-pressure, high-temperature procedure developed at the hydrocarbon recovery laboratory of the Mexican Petroleum Institute Serrano-Saldaña 2018.

The experimental setup used for these measurements is shown schematically in Figure 4. The apparatus consists of a high-pressure cell equipped with optical windows, temperature control system, and precision injection system for droplet formation and monitoring.

First, the system was conditioned and prepared for the experiment. Subsequently, the brine was injected into the cell containing a polished Bedford limestone plate. Following this, a droplet of crude oil was carefully injected onto the rock surface immersed in the brine phase. The system was then stabilized at controlled conditions of 65°C and 50 psi , with the moderate pressure serving to prevent fluid evaporation. Finally, the oil droplet was allowed to equilibrate, and high-resolution photographic images were captured for analysis. An image of the oil droplet used for contact angle determination is shown in Figure 5.

2.5.2 *Interfacial tension measurement*

The interfacial tension (IFT) between the crude oil and various brine compositions was measured using the pendant drop method within the same high-pressure, high-temperature system used for contact angle measurements as shown in Figure 4. The IFT determination was based on analysis of the shape of pendant oil droplets suspended in the brine phase.

The experimental procedure for IFT measurements consists the following steps. Initially, the IFT was measured using pendant oil droplets suspended in the brine phase without the presence of the rock substrate. Subsequently, for contact angle determination, separate oil droplets were released onto the polished rock surface and allowed to equilibrate, after which the equilibrium contact angle was measured as shown in Figure 5. Finally, to ensure measurement consistency and account for potential temporal effects, the IFT was measured again using fresh pendant droplets in the brine phase.

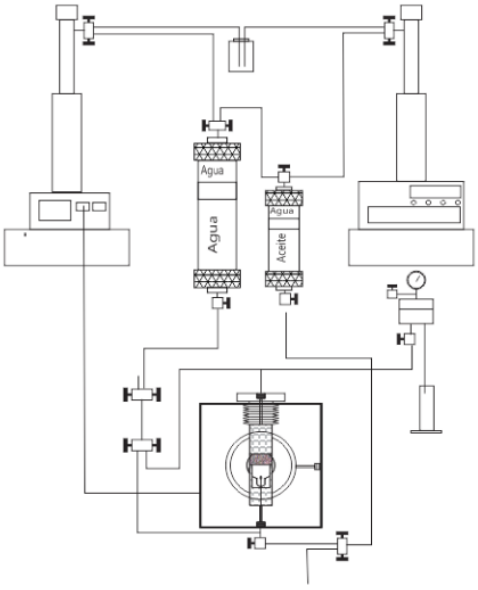

Fig. 4: Schematic of the high-pressure, high-temperature system used for measuring contact angle and interfacial tension under reservoir conditions.

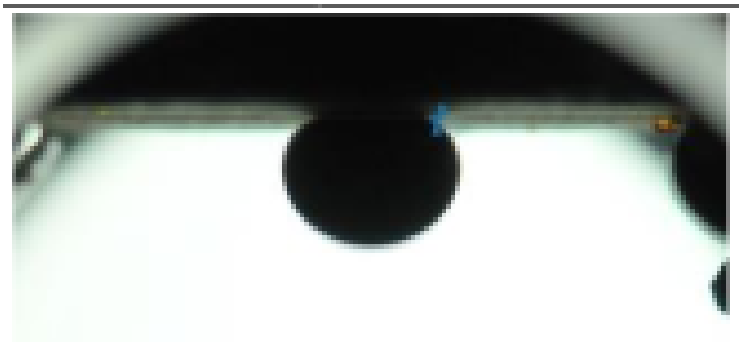

Fig. 5: Image of an oil droplet on a rock surface immersed in FW brine, used for contact angle measurement.

3 Geochemical Methodology

This study was conducted to develop a novel diagnostic tool for evaluating oil recovery from carbonate reservoirs under various brine compositions, thereby addressing a significant gap in the optimization of low salinity waterflooding process. Conventional laboratory methods, including coreflooding and spontaneous imbibition tests, are recognized for providing valuable insights; however, they are characterized by substantial time requirements, expensive, and inherent limitations in the number of brine compositions that can be evaluated.

The proposed geochemical methodology aims to provide a rapid screening alternative by quantitatively modeling the geochemical reactions at the crude oil-brine-rock interface using bond product sum calculations. It is important to note that this computational approach is predicated on data obtained from rock, brine, and oil samples. Furthermore, the methodology was validated against laboratory tests, specifically spontaneous imbibition experiments. While the acquisition of these fundamental rock and fluid properties required substantial initial investment, they provided the necessary inputs and validation basis for the rapid computational screening of numerous brine compositions.

The present work extends the theoretical framework established by Brady and Thyne (2016), Tetteh, Brady, and Ghahfarokhi (2021), Almasiyan and Mahani (2024) into a practical diagnostic tool. The procedure is outlined in Figure 6 and consists of the following steps: (1) analysis of a representative LSWF case study, including Bedford limestone characterization, laboratory experiments, and SARA analysis of the crude oil; (2) identification of Gibbs energy through chemical pseudostructure approaches; (3) establishment of a chemical reaction database

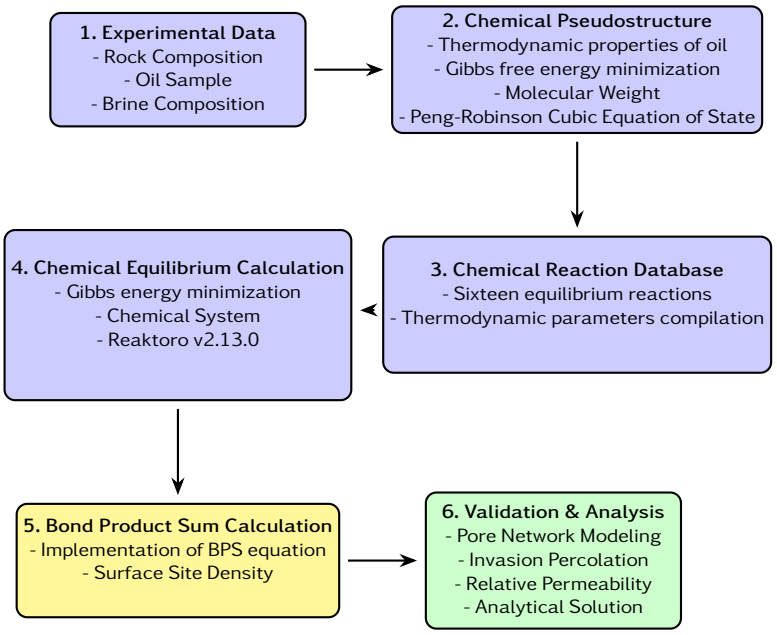

Fig. 6: Methodology Flow Diagram.

with sixteen equilibrium reactions; (4) application of chemical equilibrium calculations using Gibbs energy minimization; (5) calculation of the bond product sum as a quantitative indicator of wettability; and (6) validation of the model predictions through direct comparison with experimental imbibition data.

3.1 Experimental Data

This geochemical analysis uses experimental data from section 2: the Bedford limestone sample in table *2.1*, crude oil with properties detailed in table 2, and brine formulations with compositions given in table 3.

3.2 Chemical Pseudostructure

The chemical pseudostructure concept is widely used to represent the functional groups that characterize the chemical reactivity of an unidentifiable petroleum fraction. Following the determination of these pseudostructures via Gibbs Free Energy Minimization (GEM), balance calculations were performed to calcualte the total number of carbon and hydrogen atoms for the oil fraction. These calculations provided the necessary formation properties for subsequent chemical equilibrium analyses.

In this study, the Gibbs free energy of the oil phase was a requisite parameter for chemical equilibrium calculations. Given that the crude oil was classified as light as shown in Table 2, and the experiment were conducted at a pH 6 where carboxylic acid groups are predominantly deprotonated and are the primary reactive species at the oil-water interface the oil phase was represented by carboxylic functional groups. At this pH, surface complexation modeling demonstrates that carboxylate mineral electrostatic bridges dominate oil-rock adhesion, a behavior observed even for oils with base-to-acid number ratios (TBN/TAN) as high as 10:1 (Brady and Krumhansl 2012; Brady and Thyne 2016). Consequently, the chemical pseudostructure approach proposed by Carreón *et al.,* (2021) was adopted. This method was selected because it provides a practical and thermodynamically consistent framework for characterizing light petroleum fractions when detailed molecular compositions are unknown.

The chemical pseudostructure concept treats each petroleum fraction as a single pure component with a simplified molecular representation. According to Carreón *et al.,* (2021), this approach enables the characterization of chemical reactivity by assigning a set of functional groups to each fraction. In this work, the carboxylic acid group (-COOH) was used as the primary functional group. These pseudostructures are defined by non-integer occurrences of functional groups, denoted as υ_{ij}, where i refers to the functional group type and j to the petroleum fraction.

Gibbs Free Energy Minimization

Instead of relying on experimental critical properties which are often unavailable for heavy fractions the occurrence of functional groups υ_{ij} was determined by minimizing the Gibbs free energy. In this work, the carboxylic acid group (-COOH) was used as the primary functional group representing the chemically active polar portion of the oil. The molar Gibbs free

energy for a pure component is given by:

$$\frac{G_j^0}{RT} = \ln(\phi_j^0) + \frac{\mu_j^0}{RT} + \ln\left(\frac{P_j}{P^0}\right) \tag{1}$$

where G_j^0 is the molar Gibbs free energy, R is the universal gas constant, T is temperature, ϕ_j^0 is the fugacity coefficient, μ_j^0 is the standard-state chemical potential, P_j is the pressure, and P^0 is the reference pressure.

Under equilibrium conditions, the ideal-gas terms remain constant, simplifying the objective function to:

$$\frac{G_j^0}{RT} = \ln(\phi_j^0) \tag{2}$$

The minimization problem for the carboxylic acid functional group is then formulated as:

$$\min_{\upsilon_{\mathrm{COOH}j}} \ln(\phi_j^0) \tag{3}$$

where $\upsilon_{\mathrm{COOH}j}$ represents the occurrence of carboxylic acid groups in petroleum fraction j.

The minimization was subject to constraints based on experimental bulk properties. The molecular weight constraint was expressed as:

$$\upsilon_{\mathrm{COOH}j} M_{\mathrm{COOH}} - M_j = 0 \tag{4}$$

where M_{COOH} = 45 g/mol is the molecular weight of the -COOH group and M_j is the molecular weight of the petroleum fraction.

The mass density constraint was given by:

$$\upsilon_{\mathrm{COOH}j} \Delta v_{\mathrm{COOH}} - \frac{M_j}{\hat{\rho}_j} = 0 \tag{5}$$

where Δv_{COOH} is the volume increment of the carboxylic acid group and $\hat{\rho}_j$ is the mass density.

The hydrogen-to-carbon ratio constraint was formulated as:

$$\upsilon_{\mathrm{COOH}j}\left(\mathrm{HCR}_{\mathrm{COOH}} - \mathrm{HCR}_j\right) = 0 \tag{6}$$

where $\mathrm{HCR}_{\mathrm{COOH}}$ = 1.0 and HCR_j represent the hydrogen-to-carbon molar ratios of the carboxylic acid group and petroleum fraction, respectively.

These constraints ensured that the pseudostructure accurately reflected the experimental molecular weight, density, and elemental composition using the carboxylic acid representation.

The molecular weight of each pseudocomponent was computed as:

$$M_j = \upsilon_{\mathrm{COOH}j} M_{\mathrm{COOH}} \tag{7}$$

This equation represents a mass balance where the total molecular weight is determined by the contribution from the carboxylic acid functional groups.

Peng-Robinson Cubic Equation of State

The critical properties and functional group parameters derived from the above procedure were used within the Peng-Robinson Cubic Equation of State (CEoS), combined with appropriate mixing rules, to compute the fugacity coefficient ϕ_j^0. This methodology allowed the use of predictive mixing rules without the need for extensive adjustment of binary interaction parameters, as highlighted by Carreón *et al.,* 2021.

3.3 Chemical Reaction Database

To model the geochemical interactions at the crude oil-brine-rock interface, a comprehensive chemical reaction database was developed as the foundation for our diagnostic tool. This database comprises sixteen equilibrium reactions categorized into four distinct groups: brine phase reactions, solid-brine interface reactions, oil-brine interface reactions, and solid phase reactions. The selection of these reactions was based on the surface complexation model framework established by Brady; Brady, Bryan, *et al.,* (2011; 2016), as detailed in Table 5.

The database construction followed a methodology beginning with eight fundamental brine phase reactions that govern aqueous ionic interactions. These reactions include the dissociation of water and carbonate system equilibria, with particular focus on potential determining ions such as Mg^{2+}, Ca^{2+}, and SO_4^{2-}. The brine phase reactions directly influence the ionic distribution that subsequently interacts with both mineral and oil surfaces.

The solid-brine interface was characterized through six reactions describing calcite surface interactions. Particular attention was given to the behavior of surface sites such as >CaOH and $>CO_3H$, which play important roles in determining wettability alteration. Key reactions included protonation of surface sites and cation binding mechanisms at carbonate surfaces.

For the oil-brine interface, our study integrated three carboxylic acid reactions to represent the polar interactions of crude oil components. The fundamental reaction governing carboxylic acid dissociation is given by:

$$-\mathrm{COOH} \rightleftharpoons -\mathrm{COO}^- + \mathrm{H}^+ \tag{8}$$

This dissociation reaction was complemented by cation complexation mechanisms described by:

$$-\mathrm{COOH} + \mathrm{Ca}^{2+} \rightleftharpoons -\mathrm{COOCa}^+ + \mathrm{H}^+ \tag{9}$$

$$-\mathrm{COOH} + \mathrm{Mg}^{2+} \rightleftharpoons -\mathrm{COOMg}^+ + \mathrm{H}^+ \tag{10}$$

These oil-brine interface reactions are particularly significant as they directly influence the electrostatic

Table 5. Surface complexation reactions

No.	Reactions	$\log K_{eq}$ **at** 25°C
Brine Phase Reactions		
1	$H_2O \rightleftharpoons H^+ + OH^-$	−13.99
2	$HCO_3^- \rightleftharpoons H^+ + CO_3^{2-}$	−10.33
3	$H_2CO_3 \rightleftharpoons HCO_3^- + H^+$	−6.35
4	$MgSO_4 \rightleftharpoons Mg^{2+} + SO_4^{2-}$	−2.37
5	$NaSO_4^- \rightleftharpoons Na^+ + SO_4^{2-}$	−0.70
6	$CaSO_4 \rightleftharpoons Ca^{2+} + SO_4^{2-}$	−2.3
7	$CaCl^+ \rightleftharpoons Ca^{2+} + Cl^-$	−0.7
8	$MgCl^+ \rightleftharpoons Mg^{2+} + Cl^-$	−0.15
Solid-Brine Interface Reactions		
10	$>CaOH + H^+ \rightleftharpoons >CaOH_2^+$	11.85
11	$>CaOH_2^+ + SO_4^{2-} \rightleftharpoons >CaSO_4^- + H_2O$	2.1
12	$>CaOH + HCO_3^- \rightleftharpoons >CaCO_3^- + H_2O$	5.8
13	$>CO_3H \rightleftharpoons >CO_3^- + H^+$	−5.1
14	$>CO_3H + Ca^{2+} \rightleftharpoons >CO_3Ca^+ + H^+$	−4.4
15	$>CO_3H + Mg^{2+} \rightleftharpoons >CO_3Mg^+ + H^+$	−4.4
Oil-Brine Interface Reactions		
16	$-COOH \rightleftharpoons -COO^- + H^+$	−4.6
17	$-COOH + Ca^{2+} \rightleftharpoons -COOCa^+ + H^+$	−3.6
18	$-COOH + Mg^{2+} \rightleftharpoons -COOMg^+ + H^+$	−3.4
Solid Phase Reactions		
19	$CaCO_3(s) + H^+ \rightleftharpoons Ca^{2+} + HCO_3^-$	1.78

Note: The equilibrium constants ($\log K$) for reactions 1–8 and 16 were obtained from the SUPCRT Database, while the $\log K$ values for reactions 10–18 were obtained from Tetteh, Brady, and Ghahfarokhi (2021). The > represent the solid surface, − represents the polar oil surface groups.

interactions that control wettability alteration during Low Salinity Waterflooding.

The database was completed by including the calcite dissolution reaction to account for mineral dissolution effects:

$$CaCO_3(s) + H^+ \rightleftharpoons Ca^{2+} + HCO_3^- \qquad (11)$$

For thermodynamic characterization, a dual-database approach was implemented. Fundamental thermodynamic parameters for individual species in the brine phase were obtained from the SUPCRT Database (Johnson *et al.,* 1992), which provides comprehensive data including Gibbs free energy of formation (G_f), enthalpy of formation (H_f), standard molar entropy (S_r), molar volume (V_r), and Maier-Kelley heat capacity coefficients (a, b, c). The theoretical foundation for these thermodynamic parameters has been extensively documented in the literature (Helgeson and Kirkham 1974; Tanger and Helgeson 1988).

For the equilibrium reactions themselves, particularly those at the solid-brine and oil-brine interfaces, we adopted the established equilibrium constants (logK values), with interface reaction constants validated by Brady (2011), Brady, Krumhansl, and Mariner (2012), Brady and Krumhansl (2013), Brady and Thyne (2016) for carbonate LSWF systems. This approach guaranteed thermodynamic consistency while incorporating reaction parameters specifically relevant to LSWF processes.

The implementation of the chemical reaction database utilized Reaktoro v2.13.0, an open-source computational framework designed for modeling chemically reactive systems (Leal 2015). This platform enabled the creation of a comprehensive thermodynamic database incorporating all sixteen equilibrium reactions, providing a robust foundation for geochemical equilibrium calculations.

3.4 Chemical Equilibrium Calculation

The determination of chemical equilibrium in this study was based on the minimization of Gibbs free energy (Leal, Blunt, and LaForce 2013; Leal, Blunt, and LaForce 2014; Leal 2015), representing an alternative approach to conventional geochemical solvers that employ mass-balance methodologies (Parkhurst and Appelo 2013). It is important to note that these calculations represent static equilibrium states rather than dynamic processes, distinguishing them from the transient behavior observed in

spontaneous imbibition tests. The primary purpose of these equilibrium calculations was to provide essential input parameters for Bond Product Sum calculations.

This framework accommodates various constraint types including fixed chemical potential (μ_i = constant), pressure (P), number of moles of species i (n_i), total number of species (N), molar composition vector (**n**), temperature (T), and pH. Following Leal, Kulik, *et al.,* (2016), the equilibrium calculation is formulated as a constrained optimization problem:

$$\min_{\mathbf{n}} G(T,P,\mathbf{n}) := \sum_{i=1}^{N} n_i \mu_i(T,P,\mathbf{n}) \tag{12}$$

subject to elemental mass balance constraints:

$$\mathbf{An} = \mathbf{b} \tag{13}$$

and non-negativity constraints:

$$n_i \geq 0, \quad i = 1,\ldots,N \tag{14}$$

where **A** represents the stoichiometric matrix relating species to elements, **b** represents the vector of elemental abundances, and $\mu_i(T,P,\mathbf{n})$ signifies the chemical potential of species i. The chemical potential is expressed as:

$$\mu_i(T,P,\mathbf{n}) = \mu_i^{\circ}(T,P) + RT \ln a_i(\mathbf{n}) \tag{15}$$

where $\mu_i^{\circ}(T,P)$ represents the standard chemical potential and $a_i(\mathbf{n})$ represents the activity of species i.

A principal advantage of this methodology is its independence from specific species or phase details, enabling application to diverse chemical systems (Leal, Blunt, and LaForce 2013; Leal, Blunt, and LaForce 2014). The implementation uses a full Newton method rather than the incomplete Newton approaches used in other geochemical solvers (Parkhurst and Appelo 2013), ensuring optimal convergence rates even in highly non-linear multiphase systems.

The equilibrium calculations were conducted at a constant temperature of 65°C, pressure of 1 atm, and pH of 6, replicating the experimental conditions of spontaneous imbibition tests. All brine compositions detailed in Table 3 were systematically evaluated through separate equilibrium calculations. This approach enabled assessment of the effects of Ca^{2+}, Mg^{2+}, and SO_4^{2-} on the equilibrium state.

The computational procedure involved three steps: (1) definition of the chemical system incorporating all species from the reaction database; (2) specification of initial conditions corresponding to each brine composition; and (3) execution of the equilibrium solver followed by extraction of charged surface species concentrations. This systematic processing of multiple brine compositions provided quantitative data on brine chemistry effects on COBR surface at equilibrium. While these calculations represent static equilibrium states rather than dynamic processes, they served as crucial inputs for the subsequent BPS calculations, which form the core of our diagnostic tool for predicting wettability alterations.

3.5 Bond Product Sum Calculation

The bond product sum provides a quantitative calculation of electrostatic interactions occurring at the crude oil-brine-rock interfaces. This mechanism evaluates the strength of electrical attractions between oppositely charged surface sites across these interfaces, offering molecular-level insights into wettability characteristics of reservoir rocks. Following the chemical equilibrium calculations described in the previous section, we applied the bond product sum to evaluate how different brine compositions influence wettability alteration potential in carbonate systems.

At the molecular level, rock-brine and oil-brine interfaces exhibit complex electrostatic interactions characterized by diverse distributions of charged speciation sites. The rock-brine interface presents both cationic and anionic sites, while the oil-brine interface similarly displays positive and negative charges. Electrostatic bonds form between these oppositely charged sites across the interfaces. Specifically, positively charged sites on the rock surface attract negatively charged functional groups at the oil-brine interface, while anionic sites on the rock interact electrostatically with cationic species at the oil-water interface.

The BPS concept was initially introduced by Brady and Thyne (2016) to explain wettability alteration mechanisms in COBR systems. Tetteh, Brady, and Ghahfarokhi (2021) expanded this theoretical foundation by developing a mathematical model for BPS to quantitatively evaluate how potential determining ions affect COBR interfaces. For our investigation, we implemented the mathematical formulation proposed by Tetteh, Brady, and Ghahfarokhi (2021):

$$\begin{aligned}\mathrm{BPS} = {} & [-\mathrm{COOCa}^+][>\mathrm{CaCO_3^-}] + [-\mathrm{COOMg}^+][>\mathrm{CaCO_3^-}] \\ & + [-\mathrm{COO}^-][>\mathrm{CaOH_2^+}] + [-\mathrm{COOCa}^+][>\mathrm{CO_3^-}] \\ & + [-\mathrm{COOMg}^+][>\mathrm{CO_3^-}] + [-\mathrm{COOCa}^+][>\mathrm{CaSO_4^-}] \\ & + [-\mathrm{COOMg}^+][>\mathrm{CaSO_4^-}] + [-\mathrm{COO}^-][>\mathrm{CO_3Ca}^+] \\ & + [-\mathrm{COO}^-][>\mathrm{CO_3Mg}^+]\end{aligned} \tag{16}$$

The BPS calculation focused specifically on the carboxylic functional group (−COOH) as the primary fraction of the oil phase that reacts with the brine, rather than including nitrogenous base groups ($-NH^+$), because brines in carbonate formations tend to have a more acidic behavior, usually a pH greater

than 6. This is a well-known fact in the process of wettability alteration in carbonates (Brady, Bryan, *et al.,* 2016; Brady and Krumhansl 2012; Brady and Thyne 2016).

Surface site density values represent a critical parameter for BPS calculation. As reported by Tetteh and Barati 2019 and Almasiyan and Mahani (2024), specific surface sites including > CaOH and > CO_3H remain fundamental for accurate BPS evaluation. We adopted site density values reported by Almasiyan and Mahani (2024): 1 site/nm² for > CO_3H and 4 sites/nm² for > CaOH. These values were originally derived from Awolayo *et al.,* (2014), Mahani, Keya, Berg, and Nasralla (2016), Sanaei *et al.,* (2019) through systematic calibration of surface complexation model parameters against experimental data.

The conversion of surface density measurements to molar concentrations used from Bedford limestone specific surface area and solid concentration data presented in Table 6. This conversion was essential for integrating these values into our chemical solver and maintaining consistency across all calculations. The molar concentration of surface sites was calculated using:

$$C_{\text{site}} = \frac{\rho_{\text{site}} \times A_{\text{specific}} \times m_{\text{solid}}}{N_A} \tag{17}$$

where C_{site} represents the molar concentration of surface sites, ρ_{site} is the surface site density (sites/nm²), A_{specific} is the specific surface area (m²/kg), m_{solid} is the solid mass (kg), and N_A is Avogadro number.

This methodological approach enabled quantitative assessment of how varying brine compositions influence electrostatic interactions at COBR interfaces, providing a molecular-level understanding of wettability alteration mechanisms in low salinity waterflooding applications.

Table 6. Extra Bedford Information

Name	Amount
Specific Surface Area	290 m^2/kg
Solid concentration	0.272 kg

Note: Specific Surface Area was taken from Qiao, Li, *et al.,* (2016).

3.6 *Methodology validation*

After completing the geochemical calculations, we performed validation using three connected calculations: pore network modeling with OpenPNM software (Gostick, Aghighi, Hinebaugh, Tranter, Hoeh, Day, Spellacy, Sharqawy, Bazylak, Burns, Lehnert, and Putz 2016) to simulate fluid displacement at the pore scale, Brooks-Corey Modified correlations to link saturation data with relative permeability functions, and analytical solutions for spontaneous imbibition prediction (McWhorter and Sunada 1990). These methods provided a basis for checking the bond product sum predictions against known fluid flow behavior.

3.6.1 *Pore Network Modeling*

To include dynamic flow effects not covered by the static BPS calculations, we used a quasi-static rate-controlled pore network modeling approach with OpenPNM software Gostick, Aghighi, Hinebaugh, Tranter, Hoeh, Day, Spellacy, Sharqawy, Bazylak, Burns, Lehnert, and Putz 2016. This method simulated invasion percolation processes in Bedford limestone, showing fluid movement at the pore scale.

We began with a Bedford carbonate network from computed microtomography data, containing 1464 pores and 760 throats modeled as spheres and cylinders, as shown in Figure 7. The invasion percolation method found fluid paths using capillary entry pressures from the Washburn equation:

$$P_{c,entry} = \frac{2\sigma\cos(\theta)}{R_{i-j}} \tag{18}$$

where $P_{c,entry}$ is the capillary entry pressure for throat invasion, σ is the interfacial tension between oil and brine, θ is the contact angle, and R_{i-j} is the radius between pores i and throat j.

To get relative permeability curves for different brine compositions, we ran invasion percolation simulations.

Invasion Percolation

The relative permeability curves started with invasion percolation simulations using OpenPNM quasi-static rate-controlled method Gostick, Aghighi, Hinebaugh, Tranter, Hoeh, Day, Spellacy, Sharqawy, Bazylak, Burns, and Lehnert 2016. This approach simulated the non-wetting phase entering the initially oil-filled network by choosing the easiest throat to invade at each step, based on capillary entry pressures. The invasion followed the rule that the entering phase moves through the path with least resistance.

When a throat was invaded, the connected pore filled with the invading phase, and new throats linked to this pore became available for invasion.

Hydraulic Conductance

After each invasion step, we found the hydraulic conductance for both phases in their occupied pores. For the wetting phase, throat conductance was calculated with the Hagen-Poiseuille equation for

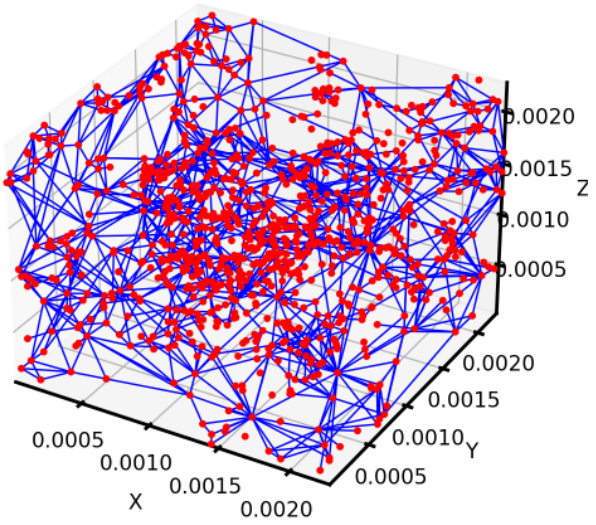

Fig. 7: Bedford Pore Network Image.

cylindrical channels:

$$Q_\alpha = \frac{\pi R_{i-j}^4 (P_i - P_j)}{8\mu_\alpha L_{i-j}} \tag{19}$$

where Q_α is the hydraulic conductance for phase α between pores i and throat j, μ_α is the viscosity of phase α, L_{i-j} is the throat length, and α represents the fluid phase oil or brine.

Relative Permeability estimation

To determine relative permeability, we first calculated absolute permeability for each phase using Darcy's law:

$$K_{abs}^\alpha = \frac{Q_{total}\mu L}{(P_{inlet} - P_{outlet})A_{cross}} \tag{20}$$

where K_{abs}^α is the absolute permeability of phase α (brine or oil), L is the network length in the flow direction, and A_{cross} is the cross-sectional area.

The relative permeability for each phase was then found as the ratio of effective permeability to absolute permeability:

$$K_{r,\alpha} = \frac{Q_{inlet}^\alpha}{K_{abs}^\alpha} \tag{21}$$

where $K_{r,\alpha}$ is the relative permeability of phase α, and Q_{inlet}^α is the inlet flow rate for Stokes flow conditions.

3.6.2 *Brooks-Corey Modified*

To validate the relative permeability data obtained through pore network modeling, we applied the Brooks-Corey Modified equation to fit the calculated results. This approach allowed us to establish empirical relationships between saturation data and relative permeability functions for different brine compositions.

Normalized Water Saturation

The normalization of water saturation converted the raw saturation data from pore network modeling into a standardized scale that represents the actual flowing saturation range. The normalized water saturation S_e was calculated from the measured water saturation S_w using:

$$S_e = \frac{S_w - S_{wr}}{1 - S_{wr} - S_{or}} \tag{22}$$

where S_e is the normalized water saturation, S_w is the measured water saturation, S_{wr} is irreducible water saturation, and S_{or} is the residual oil saturation.

Modified Brooks-Corey Model

The Modified Brooks-Corey model provided mathematical expressions for relative permeability behavior in two-phase systems. For the wetting phase (water), the relative permeability was expressed as:

$$k_{rw}(S_e) = k_{rw}^0 \cdot S_e^{n_w} \tag{23}$$

For the non-wetting phase (oil), the relative permeability was defined as:

$$k_{ro}(S_e) = k_{ro}^0 \cdot (1 - S_e)^{n_o} \tag{24}$$

where k_{rw}^0 and k_{ro}^0 represent the endpoint relative permeability for water and oil respectively, and the Corey exponents n_w and n_o control the curvature of the relative permeability curves, reflecting pore structure characteristics and fluid distribution.

Initial Parameter Selection for Curve Fitting

In this study, the values were selected as initial guesses for all fitting parameters: $k_{rw,0} = 1$, $n_{w,0} = 1$, $k_{ro,0} = 1$, and $n_{o,0} = 1$. The selection of consistent initial values across all experiments was designed to maintain consistency in the fitting procedure and allow for useful comparison of fitted parameters between different experimental conditions. This standardization enhances the reliability of comparative analyses between various brine compositions and their effects on relative permeability behavior.

3.6.3 Analytical Solution

This study applies the McWhorter and Sunada (1990) analytical solution to model one-dimensional countercurrent two-phase flow with capillary effects. The solution provides a mathematical framework for predicting spontaneous imbibition behavior, which was validated using the Ls2 limestone case study.

Governing Equations

The water saturation distribution during spontaneous imbibition is described by:

$$\phi \frac{\partial S_w}{\partial t} + u \frac{df_w}{dS_w} \frac{\partial S_w}{\partial x} - \frac{\partial}{\partial x}\left(D(S_w) \frac{\partial S_w}{\partial x} \right) = 0 \quad (25)$$

where ϕ is porosity, S_w is water saturation, t is time, u is total velocity, f_w is water fractional flow, and x is the spatial coordinate. The capillary diffusion coefficient $D(S_w)$ is defined as:

$$D(S_w) = -\frac{k k_{nw} f}{\mu_{nw}} \frac{dp_c}{dS_w} \quad (26)$$

where k is absolute permeability, k_{nw} is nonwetting phase relative permeability, μ_{nw} is nonwetting phase viscosity, and p_c is capillary pressure.

The fractional flow function for water is given by:

$$f(S_w) = \left(1 + \frac{k_{nw}\mu_w}{k_w \mu_{nw}} \right)^{-1} \quad (27)$$

where k_w is water relative permeability and μ_w is water viscosity.

Boundary and Initial Conditions

The initial condition assumes the porous medium is saturated with oil at residual water saturation:

$$S_w(x,0) = S_i = S_{wr} \quad (28)$$

The inlet boundary condition specifies the water injection rate:

$$q_0 = q_w(0,t) = At^{-1/2} \quad (29)$$

where A is a constant characterizing injection strength. The boundary condition at infinity ensures that the disturbance does not reach the far end of the domain:

$$S_w(\infty, t) = S_i \quad (30)$$

Relative Permeability Functions

The effective water saturation is calculated as:

$$S_e = \frac{S_w - S_{wr}}{1 - S_{wr} - S_{or}} \quad (31)$$

where S_{wr} is irreducible water saturation and S_{or} is residual oil saturation. The relative permeability functions are:

$$k_{ro}(S_w) = (1 - S_e)^2 \left(1 - S_e^{(2+\theta)/\theta} \right) \quad (32)$$

$$k_{rw}(S_w) = S_e^{(2+3\theta)/\theta} \quad (33)$$

where θ is the Brooks-Corey pore-size distribution parameter.

Recovery Factor Calculation

The cumulative water injection volume is obtained by integrating the injection rate:

$$Q_w(t) = \int_0^t At^{-1/2} dt = 2A\sqrt{t} \quad (34)$$

The recovery factor is then calculated as:

$$\text{Recovery Factor } (\%) = \min\left(\frac{Q_w(t)}{V_{o0}}, R_{max} \right) \times 100 \quad (35)$$

where V_{o0} is initial oil volume and R_{max} is maximum theoretical recovery.

4 Spontaneous imbibition test results

The results of oil recovery for each injection stage with different formulations of brine composition from the spontaneous imbibition experiments, conducted at 65°C on Bedford limestone core samples, are summarized in Figure 8. The brine compositions used in these tests are detailed in Table 3. The experimental design was structured to systematically evaluate the impact of modification in brine composition on oil recovery.

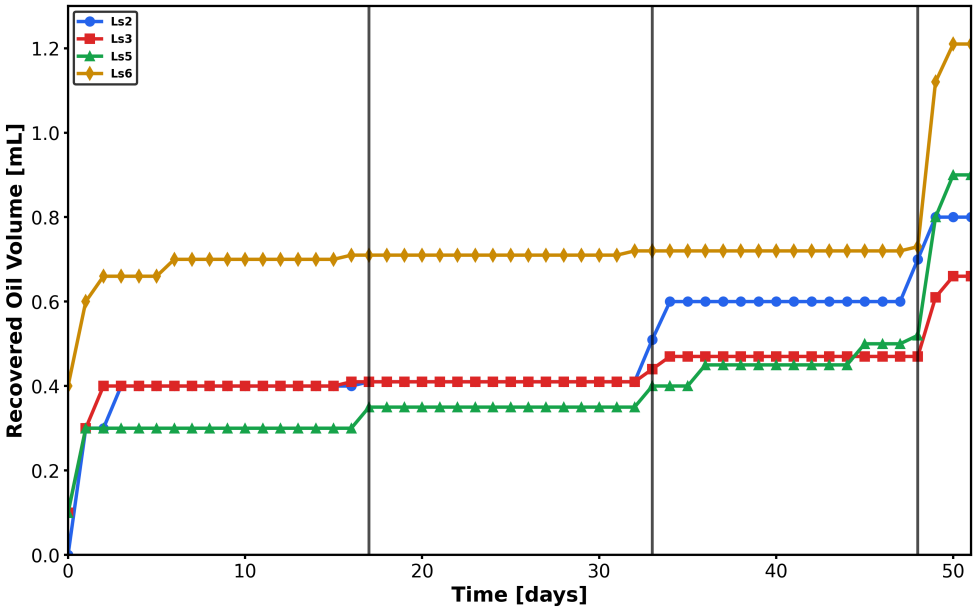

Fig. 8: Spontaneous imbibition tests at 65 °C for Bedford limestone samples.

A common trend was observed in the initial stages of all tests: a decreased in Total Dissolved Solids for each brine composition was correlated with an increase in oil recovery. This finding is consistent with a wettability alteration toward a more water-wet state caused by lower salinity.

The effect of potential determining ions was also investigated. The transition from FW/2 to FW/2 + $MgSO_4$ in sample Ls2, which involved the addition of both Mg^{2+} and SO_4^{2-}, resulted in a slight increase in oil recovery. This effect showed that the presence of these ions are effective in promoting wettability alteration. It is important to note that the individual effects of SO_4^{2-} or Mg^{2+} alone were not isolated in this experimental design; the brines were formulated to evaluate their combined impact.

A more noticeable effect was observed in stages where the Mg^{2+}/Ca^{2+} ratio was more favorable. For instance, the stage adding $MgSO_4$ in samples Ls5 and Ls6, which started from a lower salinity (FW/4), resulted in an increase in oil recovery. This suggests that the combination of Mg^{2+} and SO_4^{2-} effectively disrupts the equilibrium at the crude oil-brine-rock interface, and its efficacy is enhanced at lower overall salinities.

The most significant recovery was achieved with the introduction of modified seawater brines (SW6 and SW7). The performance of SW6, for example, can be connected to its specific ionic composition. While its sulfate concentration is comparable to the $MgSO_4$ brines, its defining characteristic is a high Mg^{2+}/Ca^{2+} ratio coupled with a low total salinity. This specific composition appears to be optimal for enhancing the interactions at the COBR interface. These findings suggest that the coupling between Mg^{2+} and SO_4^{2-} is critical for achieving higher oil recovery, and that the natural ion content of seawater provides favorable oil recovery performance.

While studies by Ligthelm *et al.,* (2009), Austad *et al.,* (2012) demostrated that sulfate adsorption as a primary mechanism, our results indicate that this process is contingent upon the presence of other ions, particularly Mg^{2+}. Thus, the hypothesis that SO_4^{2-} ions alone are the dominant factor is not supported by our results. The reactivity of Mg^{2+} ions with carbonate surfaces, especially in the presence of sulfate, as reported by Sakuma *et al.,* (2014), Kwak *et al.,* (2014), Generosi *et al.,* (2016), is consistent with the significant recovery increases observed in our tests when both ions are present.

5 Contact angle and interfacial tension results

Complementary measurements of contact angle and interfacial tension at 65°C were performed to provide further insight into the fluid-fluid and rock-fluid interactions. The results are summarized in Table 7.

Table 7. Contact Angle and Interfacial Tension at 65°C

	Contact Angle (°)		Interfacial Tension (mN/m)	
Brine Composition	**Value**	**Unc.**	**Value**	**Unc.**
FW	28.0	± 1.5	26.3	± 0.5
FW/2	32.2	± 1.5	25.6	± 0.5
FW/2 + $MgSO_4$	30.2	± 1.5	23.1	± 0.5
FW/4	31.0	± 1.0	24.5	± 0.5
FW/4 + $MgSO_4$	33.0	± 1.0	22.5	± 0.5
SW6	28.7	± 1.5	21.6	± 0.5
SW7	45.7	± 1.5	19.8	± 0.5

The contact angle data, a direct indicator of wettability, revealed different trends. Within the formation water, the addition of $MgSO_4$ was observed to reduce the contact angle, moving the system toward a more water-wet state. For instance, the addition to the FW/2 brine reduced the angle from 32.2° to 30.2°. This trend was consistent with the enhanced oil recovery noted in the imbibition tests and supports the role of these potential determining ions in wettability alteration. However, a different behavior was noted for the most diluted seawater brine (SW7), where the contact angle increased significantly to 45.7°. This divergence highlights that the wettability alteration is not a function of salinity alone but by the specific ionic composition and interactions within each brine.

Simultaneously, the IFT measurements showed a consistent decline across the entire brine modification sequence. The IFT decreased from 26.3 mN/m for FW to 19.8 mN/m for SW7. A notable reduction was consistently observed with the addition of $MgSO_4$, as evidenced by the IFT drops from 25.6 to 23.1 mN/m for the FW/2 series and from 24.5 to 22.5 mN/m for the FW/4 series. This indicates that the combination of Mg^{2+} and SO_4^{2-} plays a key role in modifying the crude oil-brine interface. It is important to note that the benefit of dilution was apparent even within the seawater series (from SW6 to SW7), where IFT decreased from 21.6 to 19.8 mN/m despite a reduction in both Mg^{2+} and SO_4^{2-} concentrations.

These experimental findings align well with established literature on carbonate surface interactions. Previous studies by Brady and Krumhansl (2012), Austad *et al.,* (2012), Mwangi *et al.,* (2018), Ligthelm *et al.,* (2009) have demonstrated that Mg^{2+} showed greater surface reactivity with carbonate rocks compared to Ca^{2+}. The adsorption mechanism involves Mg^{2+} and Ca^{2+} ions modifying the surface charge, while SO_4^{2-} adsorption shifts the surface charge toward more negative values. Our results corroborate the observations of Austad *et al.,* (2012), Ligthelm *et al.,* (2009), confirming that the combined presence of magnesium and sulfate enhances the reactivity at the carbonate surface. The complex behavior observed between the FW and SW series can be attributed to their different brine composition.

6 Bond product sum and ionic strength results

6.1 *Bond product sum*

The bond product sum was calculated to quantify the equilibrium electrostatic interactions at the crude oil-brine-rock interface for the various brine compositions. These calculations were performed under static, equilibrium conditions, providing a rapid assessment of wettability state without the computational expense of dynamic simulation. The BPS values, representing the electrostatic bond strength for each brine, are presented in Table 8.

Table 8. Bond Product Sum and Ionic Strength at 65 °C

Brine Composition	**BPS (mol/m²)²**	**Ionic Strength (mol/kg)**
FW	1.76×10^{-10}	2.66
FW/2	1.74×10^{-10}	1.42
FW/2 + $MgSO_4$	1.54×10^{-10}	1.43
FW/4	1.40×10^{-10}	0.85
FW/4 + $MgSO_4$	1.35×10^{-10}	0.85
SW6	1.26×10^{-10}	0.70
SW7	8.58×10^{-11}	0.61

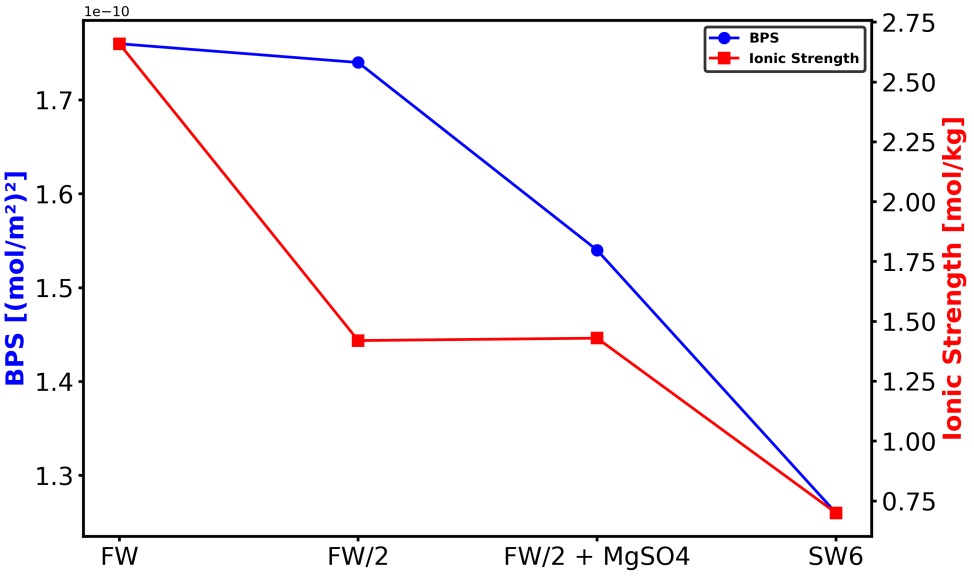

Fig. 9: Bond Product Sum and Ionic Strength at 65 °C for Ls2.

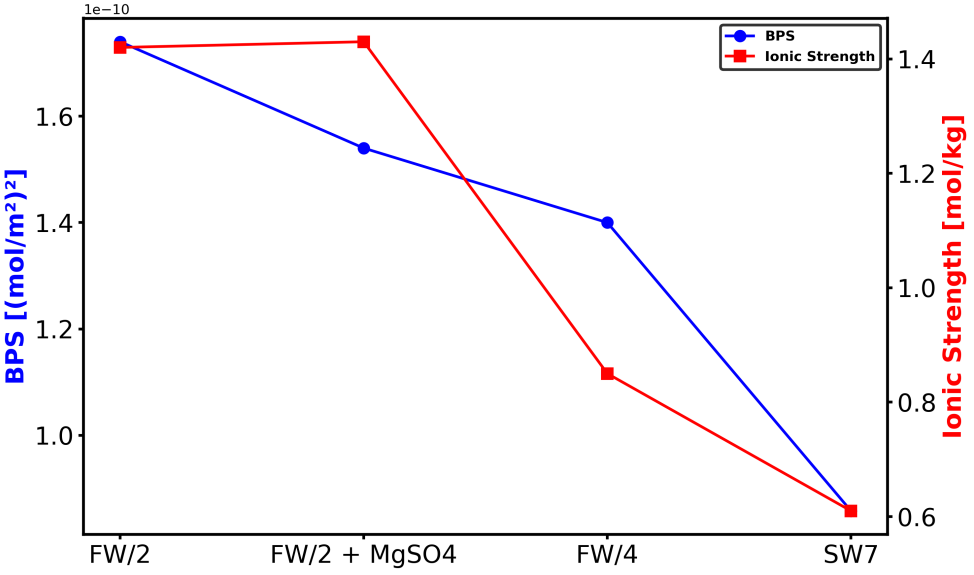

Fig. 10: Bond Product Sum and Ionic Strength at 65 °C for Ls3.

The most striking result to emerge from the data is the consistent decrease in BPS values as the brine composition transitions from formation water to modified seawater brines. This progressive reduction demonstrates a weakening of electrostatic attraction at the COBR interface. Of particular interest is the decrease observed with the SW7 brine, which showed the lowest BPS value (8.58×10^{-11} (mol/m²)²).

This trend is visually demonstrated in Figures 9 through 12, where the BPS values for each core sample consistently decrease across their respective brine sequences. The correlation between reduced BPS values and improved oil recovery observed in the spontaneous imbibition tests is evident. The most significant BPS reduction was achieved with seawater based brines (SW6 and SW7), which contained higher Mg^{2+}/Ca^{2+} ratios, providing quantitative evidence for their effectiveness in altering interfacial interactions.

Our BPS results confirm previous findings by Brady and Thyne (2016) and Chen *et al.,* (2018), who established that lower BPS values indicate weakened electrostatic bonds between oil and rock surfaces. As demonstrated by Almasiyan and Mahani (2024), this weakening of bonds facilitates the release of oil from the rock surface, thereby enhancing recovery efficiency. The clear downward trend in BPS values for all samples shows a direct relationship between reduced BPS and improved oil recovery.

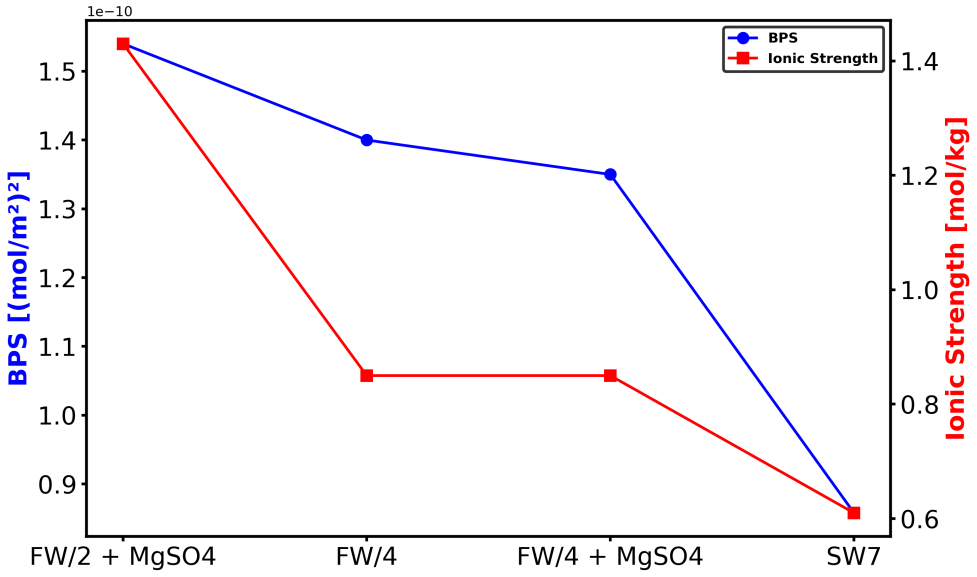

Fig. 11: Bond Product Sum and Ionic Strength at 65 °C for Ls5.

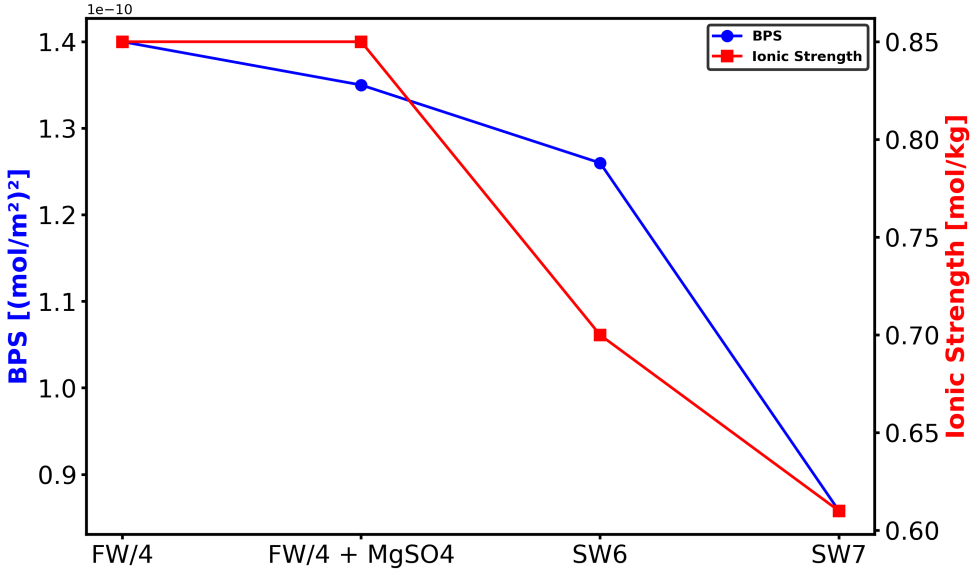

Fig. 12: Bond Product Sum and Ionic Strength at 65 °C for Ls6.

6.2 Ionic strength

The ionic strength values calculated for the tested brine compositions at 65°C are presented in Table 8. A general decreasing trend in ionic strength is observed from FW (2.66 mol/kg) to SW7 (0.61 mol/kg), which aligns with the reduction in total dissolved solids and appears to correlate with the improvement in oil recovery.

However, a more detailed analysis reveals significant discrepancies from ionic strength as a predictive parameter for wettability alteration. In several key transitions, an increase in ionic strength was accompanied by improved oil recovery.

The addition of $MgSO_4$ resulted in increased ionic strength across all core samples. Specifically, the transition to brine containing $MgSO_4$ elevated ionic strength from 1.42 to 1.43 mol/kg in Ls2 (FW/2), with a similar trend observed in Ls3 under identical conditions. Likewise, samples Ls5 and Ls6, subjected to the FW/4 to FW/4 + $MgSO_4$ transition, also exhibited increased ionic strength.

This apparent contradiction suggests that BPS offers a more sensitive measure than ionic strength for predicting LSWF performance in carbonate systems, as it captures the specific ion interactions that control wettability alteration. The results presented in Table 8 indicate that the specific chemical interactions of potential determining ions (Mg^{2+}, SO_4^{2-}) at the COBR interface exert a more dominant influence on wettability alteration than the non-

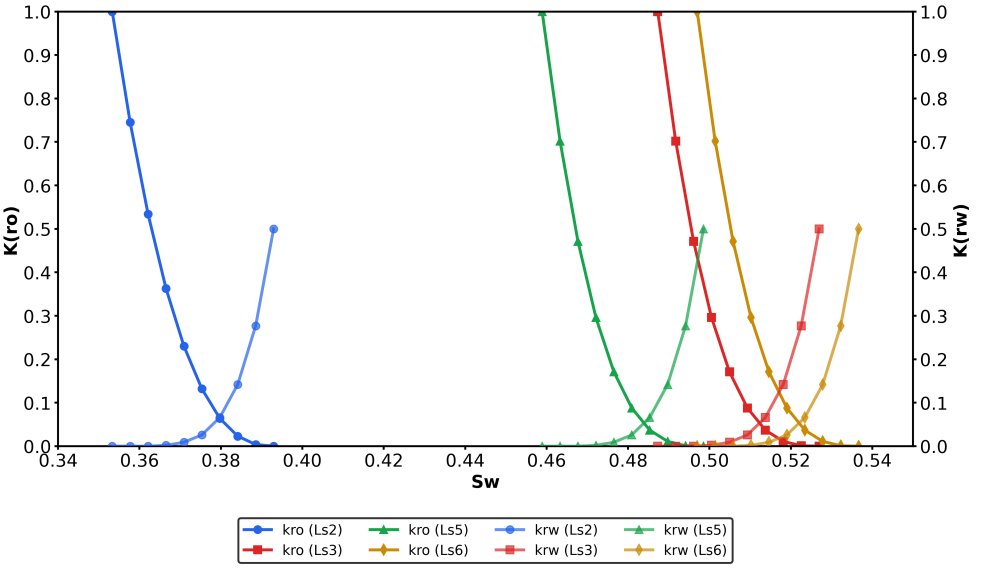

Fig. 13: Relative permeability curves for Ls2, Ls3, Ls5, and Ls6 core samples.

specific electrostatic effects described by bulk ionic strength. The demonstrated ability of Mg^{2+} and SO_4^{2-} to modify the COBR interface and enhance oil recovery, even in cases where ionic strength slightly increases, challenges the conventional idea that ionic strength alone is a sufficient parameter for oil recovery processes.

7 Methodology validation for the Ls2 case study

7.1 Initial relative permeability curves

The relative permeability curves presented in Figure 13 represent the relative permeability curves characterizing the oil and water phase flow during initial imbibition stages for four core samples (Ls2, Ls3, Ls5, Ls6). These curves were formed using the Corey model with parameters derived from experimental data. The core properties and experimental conditions are summarized in Table 1, showing variations in length (6.86–6.92 cm), diameter (3.50–3.71 cm), porosity (14.8–15.6%), pore volume (10.1–11.6 mL), absolute permeability (16.8–33.3 mD), and initial water saturation (35.3–49.7%).

The most striking result to emerge from the data is the distinct wetting behavior exhibited by each sample. Ls2 shows strong water-wet characteristics, by a pronounced decrease in oil relative permeability with increasing water saturation. This finding is consistent with its Corey (n_o = 2.5, n_w = 5.0), which fall within the established water-wet range (McPhee *et al.*, 2015). Ls3 demonstrates intermediate-wet behavior, characterized by a more moderate decline in oil relative permeability. This observation is supported by its higher initial water saturation (48.7%) and the highest absolute permeability (33.3 mD), suggesting a well-connected pore network. Ls5 exhibits transitional characteristics, with oil relative permeability behavior similar to Ls3, intermediate initial water saturation (45.9%), and moderate absolute permeability (25.2 mD), collectively indicating a mixed pore-size distribution. Of particular interest is Ls6, which presents the most favorable imbibition characteristics with the highest initial water saturation (49.7%), largest pore volume (11.6 mL), and good absolute permeability (28.5 mD). Consequently, its relative permeability curves indicate the potential for the highest oil recovery.

Having established the experimental relative permeability behavior across all core samples, we selected Ls2 as the focus for subsequent methodology validation due to the comprehensive dataset available for this sample. Pore network modeling was then employed to investigate the underlying pore-scale mechanisms controlling the macroscopic flow properties observed in this representative water-wet system.

Table 9. Predicted oil recovery parameters from relative permeability models for Ls2

Parameter	**FW**	**FW/2**	**FW/2 +** $MgSO_4$	**SW6**
S_{wr}	0.00230	0.00190	0.00120	0.00110
S_{or}	0.151	0.146	0.140	0.110
$k_{rw,0}$	0.849	0.681	0.756	0.604
n_w	4.81	5.28	5.91	6.37
$k_{ro,0}$	1.01	1.03	0.995	0.999
n_o	2.15	1.76	1.76	1.88

7.2 Relative permeability estimation using a pore network model

Pore network modeling was used to simulate fluid displacement and predict relative permeability curves for the Ls2 case. The raw data obtained from OpenPNM simulations were processed using the modified Brooks-Corey model, as detailed in Section *3.6*.1. To derive the relative permeability parameters, the water saturation was first normalized, and an initial parameter selection for curve fitting was applied. The resulting fitted parameters for each brine composition are presented in Table 9.

A progressive decreased in both the irreducible water saturation (S_{wr}) and the residual oil saturation (S_{or}) was observed from the FW to the SW6 brine. Notably, the SW6 composition achieved the lowest S_{or} value of 0.110, which corresponds to a 27% reduction compared to the FW brine. This decrease is a direct indicator of enhanced displacement efficiency.

These modeling results were in good agreement with the experimental spontaneous imbibition test. The relative permeability curves generated from the fitted parameters in Figure 14, clearly shows the curve for the SW6 brine, with the highest oil recovery.

To further evaluate the displacement efficiency, invasion percolation simulations were performed across the different brine compositions. The simulations, which modeled the advancement of the brine phase into an oil-saturated network using capillary entry pressures derived from experimental data, provided detailed saturation profiles. However, while the pore network modeling yielded critical insights into endpoint saturations and relative permeability curves, it did not calculate the cumulative oil recovery over time.

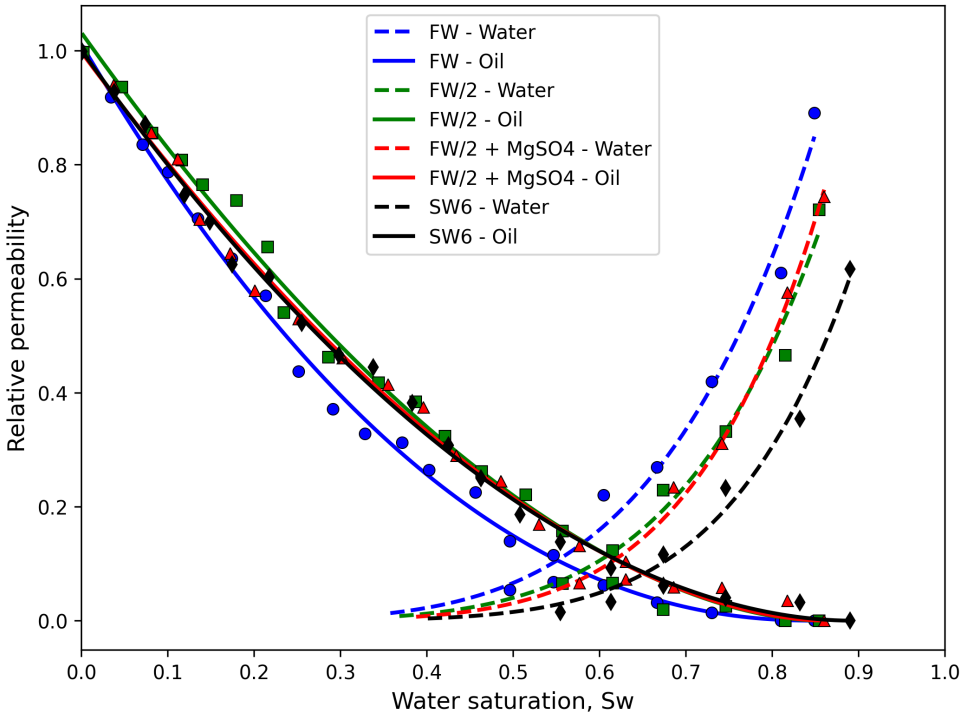

Fig. 14: Relative Permeability for Oil Recovery Prediction: Ls2

Table 10. Modified Brooks-Corey parameters for Ls2

Parameter	**FW**	**FW/2**	**FW/2 +** $MgSO_4$	**SW6**
S_{wr}	0.30	0.30	0.25	0.20
S_{or}	0.62	0.60	0.55	0.45
$k_{rw,0}$	0.80	0.81	0.85	0.65
$k_{ro,0}$	0.45	0.46	0.42	0.25
n_w	3	3	3	5
n_o	2	5	2	2

In the following subsection, the McWhorter and Sunada 1990 analytical solution is applied to incorporate these capillary drive effects and provide direct quantitative predictions of spontaneous imbibition performance.

7.3 Fitting parameters of the modified Brooks-Corey model

The modified Brooks-Corey parameters presented in Table 10 were determined through trial and error to best fit the experimental data.

The analysis revealed a progressive improvement in recovery potential across the brine composition sequence. A substantial reduction in residual oil saturation (S_{or}) was observed, decreasing from 0.62 for formation water to 0.45 for the SW6 brine composition, representing a 27.4% increase in recoverable oil. Concurrently, irreducible water saturation (S_{wr}) was found to decrease from 0.30 to 0.20, indicating enhanced fluid mobility within the porous medium as brine composition was optimized.

Figure 15 demonstrates several patterns in the spontaneous imbibition process. The most striking result to emerge from the recovery curves was the progressive enhancement in oil recovery efficiency as brine composition was optimized from formation water to seawater based composition (SW6).

The experimental data revealed that all brine compositions showed similar characteristic spontaneous imbibition behavior, with an initial rapid recovery phase followed by a gradual approach to average values. However, significant differences were observed in recovery between different brine formulations. The formation water (FW) showed the most limited recovery profile, reaching an ultimate recovery of approximately 35% of original oil in place after 15 days.

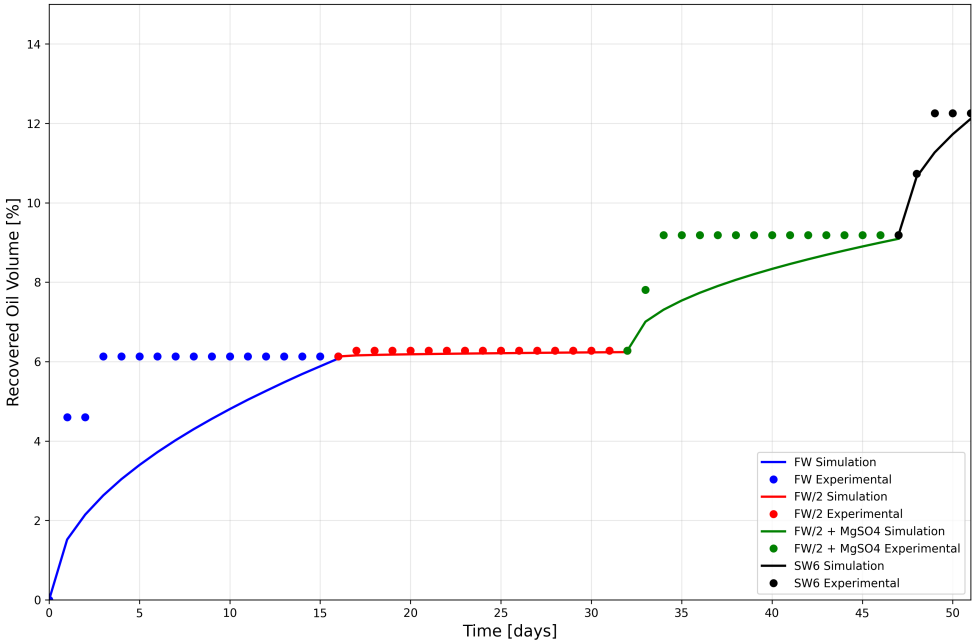

Fig. 15: Comparison of experimental oil recovery data with the fitted Modified Brooks-Corey model for core Ls2, showing recovery behavior across different brine compositions.

A notable improvement was observed with the diluted formation water (FW/2), which achieved approximately 5% higher ultimate recovery compared to the base case. The addition of $MgSO_4$ to the diluted formation water further enhanced the recovery behavior, with the FW/2 + $MgSO_4$ composition demonstrating both faster imbibition recovery.

The progressive improvement in recovery from FW to SW6 clearly demonstrates the effectiveness of optimized brine compositions in enhancing spontaneous imbibition efficiency. The SW6 composition achieved the highest ultimate recovery, which is consistent with the bond product sum calculations and pore network modeling results presented previously, confirming the multi-scale validation of the brine optimization approach.

8 Conclusions

This study successfully extended the theoretical framework of the Bond Product Sum into a practical diagnostic tool for optimizing low salinity waterflooding in carbonate reservoirs. Our integrated methodology, which combined geochemical equilibrium calculations with pore network modeling, Brooks-Corey correlations, and analytical solutions, provided a rapid and effective means of predicting wettability alteration and oil recovery performance.

As the data in Table 8 demonstrates, the most striking result was the consistent inverse relationship between BPS values and oil recovery. As brine compositions went from formation water to seawater, BPS values decreased from 1.805×10^{-9} mol/m^2 to 1.753×10^{-9} mol/m^2. This quantitative reduction in electrostatic attraction at the crude oil-brine-rock interface strongly align with enhanced oil recovery observed in spontaneous imbibition tests, confirming previous findings by Brady and Thyne 2016 and others. Our results are in good agreement with spontaneous imbibition data and fluid flow simulations, which showed a marked 27% reduction in residual oil saturation for the most effective brine composition (SW6).

Despite these results, our work clearly has some limitations. The diagnostic tool was developed and validated using a specific crude oil and Bedford limestone samples. Consequently, the findings might not be fully generalizable to all carbonate lithologies or crude oil types without further calibration. Future work should therefore concentrate on validating this methodology across a wider range of reservoir rocks and crude oils.

In conclusion, this study provides a novel and efficient methodology for screening optimal brine compositions, representing a significant advancement in geochemistry based enhanced oil recovery. By bridging the gap between molecular scale BPS calculations and macroscopic recovery predictions, our diagnostic tool offers a viable alternative to time consuming and costly laboratory experiments. We believe that our findings could be useful for designing more effective LSWF process.

Future work should integrate field-scale validation and extend the model to multicomponent systems under dynamic flow conditions.

Acknowledgements

The authors would like to acknowledge the support provided by the Consejo Nacional de Humanidades, Ciencia y Tecnología (CONAHCYT), the Mexican Petroleum Institute (IMP) project D.61057 of the Gerencia de Ingeniería de Recuperación Adicional and the Deanship of Research (DR) at King Fahd University of Petroleum & Minerals (KFUPM) for partially funding this work through Research with Humanity Microgrant Project No. RHM24102.

References

Alghamdi, A. O., Abdulaziz, K., Alotaibi, M. B., Aramco, S., & Yousef, A. A. (2017). Interaction of ionic species with calcite and oil components in waterflooding-theoretical study. *The National IOR Centre of Norway*, 24–27. https://doi.org/10.3997/2214-4609.201700269

Almasiyan, P., & Mahani, H. (2024). A bond-product-sum (bps) approach for modeling wettability alteration and enhanced oil recovery by engineered salinity waterflooding in carbonate rocks. *Energy and Fuels*, *38*, 5007–5021. https://doi.org/10.1021/acs.energyfuels.3c05055

Alvarado, V., Bidhendi, M., Garcia-Olvera, G., Morin, B., & Oakey, J. S. (2014). Spe-169127-ms interfacial visco-elasticity of crude oil-brine: An alternative eor mechanism in smart waterflooding. *SPE Improved Oil Recovery Symposium.*, 12–16. https://doi.org/10.2118/169127-ms

Austad, T., Shariatpanahi, S. F., Strand, S., Black, C., & Webb, K. J. (2012). Conditions for a low-salinity enhanced oil recovery (eor) effect in carbonate oil reservoirs. *Energy and Fuels*, *26*, 569–575. https://doi.org/10.1021/ef201435g

Awolayo, A., Sarma, H., & AlSumaiti, A. M. (2014). A laboratory study of ionic effect of smart water for enhancing oil recovery in carbonate reservoirs. *SPE EOR Conference at Oil and Gas West Asia*, SPE-169662–MS. https://doi.org/10.2118/169662-MS

Brady, P. V., Krumhansl, J. L., & Mariner, P. E. (2012). Surface complexation modeling for improved oil recovery. *Proceedings - SPE Symposium on Improved Oil Recovery*, *1*, 376–385. https://doi.org/10.2118/153744-ms

Brady, P. V., & Krumhansl, J. L. (2013). Surface complexation modeling for waterflooding of sandstones. *SPE Journal*, *18*, 214–218. https://doi.org/10.2118/163053-PA

Brady, P. V. (2011). *Why oil sticks to limestone* (tech. rep.). Sandia National Laboratories.

Brady, P. V., Bryan, C. R., Thyne, G., & Li, H. (2016). Altering wettability to recover more oil from tight formations. *Journal of Unconventional Oil and Gas Resources*, *15*, 79–83. https://doi.org/10.1016/j.juogr.2016.05.004

Brady, P. V., & Krumhansl, J. L. (2012). A surface complexation model of oil-brine-sandstone interfaces at 100°c: Low salinity waterflooding. *Journal of Petroleum Science and Engineering*, *81*, 171–176. https://doi.org/10.1016/j.petrol.2011.12.020

Brady, P., & Thyne, G. (2016). Functional wettability in carbonate reservoirs. *Energy and Fuels*, *30*, 9217–9225. https://doi.org/10.1021/acs.energyfuels.6b01895

Buckley, J. S., Liu, Y., & Monsterleet, S. (1998). Mechanisms of wetting alteration by crude oils. *SPE Journal*, *3*, 54–61. https://doi.org/10.2118/37230-PA

Carreón, B., Verónica, C., Juan, U.-V., & Aguayo, P. (2021). *Petroleum engineering thermophysical properties of heavy petroleum fluids*. http://www.springer.com/series/15095

Chandrasekhar, S., & Mohanty, K. K. (2013). Spe 166280 wettability alteration with brine composition in high temperature carbonate reservoirs. *SPE Annual Technical Conference and Exhibition*. https://doi.org/10.2118/166280-ms

Chen, Y., Xie, Q., Sari, A., Brady, P. V., & Saeedi, A. (2018). Oil/water/rock wettability: Influencing factors and implications for low salinity water flooding in carbonate reservoirs. *Fuel*, *215*, 171–177. https://doi.org/10.1016/j.fuel.2017.10.031

Dang, C. T. Q. (2013). State-of-the art low salinity waterflooding for enhanced oil recovery. *SPE Asia Pacific Oil, Gas Conference and Exhibition*, 1–12. https://doi.org/10.2118/165903-ms

Deng, X., Tariq, Z., Murtaza, M., Patil, S., Mahmoud, M., & Kamal, M. S. (2021). Relative contribution of wettability alteration and interfacial tension reduction in eor: A critical review. *Journal of Molecular Liquids*, *325*, 1–18. https://doi.org/10.1016/j.molliq.2020.115175

Derkani, M. H., Fletcher, A. J., Abdallah, W., Sauerer, B., Anderson, J., & Zhang, Z. J. (2018). Low salinity waterflooding in carbonate reservoirs: Review of interfacial mechanisms. *Colloids and Interfaces*, *2*. https://doi.org/10.3390/colloids2020020

Erzuah, S., Fjelde, I., & Omekeh, A. V. (2017). Wettability estimation by surface complexation simulations [SPE-185767-MS]. *SPE Europee featured at 79th EAGE Conference and Exhibition*.

Gachuz-Muro, H. (2013). Effects of brine on crude oil viscosity at different temperature and brine composition-heavy oil/water interaction. *SPE Europec*, 1–13. https://doi.org/10.2118/164910-ms

Gachuz-Muro, H., & Sohrabi, M. (2014). Smart water injection for heavy oil recovery from naturally fractured reservoirs. *Society of Petroleum Engineers*, 857–876. https://doi.org/10.2118/171120-ms

Gachuz-Muro, H., & Sohrabi, M. (2017). Prediction, control and validation of rock dissolution during smart water injection and its impact on waterflood performance in heavy oil carbonate reservoirs.

Generosi, J., Ceccato, M., Andersson, M., Hassenkam, T., Dobberschütz, S., Bovet, N., & Stipp, S. (2016). Calcite wettability in the presence of dissolved mg2+ and so42-. *Energy and Fuels*, *31*. https://doi.org/10.1021/acs.energyfuels.6b02029

Gostick, J., Aghighi, M., Hinebaugh, J., Tranter, T., Hoeh, M., Day, H., Spellacy, B., Sharqawy, M., Bazylak, A., Burns, A., & Lehnert, W. (2016). Openpnm: A pore network modeling package [Computing in Science and Engineering, 18(4):60–74].

Gostick, J., Aghighi, M., Hinebaugh, J., Tranter, T. G., Hoeh, M. A., Day, H., Spellacy, B., Sharqawy, M. H., Bazylak, A., Burns, A., Lehnert, W., & Putz, A. (2016). OpenPNM: A pore network modeling package. *Computing in Science & Engineering*, *18*(4), 60–74. https://doi.org/10.1109/MCSE.2016.49

Helgeson, H. C., & Kirkham, D. H. (1974). Theoretical prediction of the thermodynamic

behavior of aqueous electrolytes at high pressures and temperatures: II. Debye-Huckel parameters for activity coefficients and relative partial molal properties. *American Journal of Science*, *274*(10), 1199–1261. https://doi.org/10.2475/ajs.274.10.1199

Johnson, J. W., Oelkers, E. H., & Helgeson, H. C. (1992). SUPCRT92: A software package for calculating the standard molal thermodynamic properties of minerals, gases, aqueous species, and reactions from 1 to 5000 bar and 0 to 1000 c. *Computers & Geosciences*, *18*(7), 899–947. https://doi.org/10.1016/0098-3004(92)90029-Q

Korrani, A. K. N., Fu, W., Sanaei, A., & Sepehrnoori, K. (2015). Mechanistic modeling of modified salinity waterflooding in carbonate reservoirs. *Proceedings - SPE Annual Technical Conference and Exhibition*, *2015-Janua*, 5475–5495. https://doi.org/10.2118/175102-ms

Kwak, H. T., Yousef, A. A., Al-Saleh, S., & Aramco, S. (2014). Spe-169112-ms new insights on the role of multivalent ions in water-carbonate rock interactions.

Lager, A., Webb, K., Black, C., Singleton, M., & Sorbie, K. (2006). Low salinity oil recovery-an experimental investigation. *International Symposium of the Society of Core Analysts*, 1–13. https://www.researchgate.net/publication/241783001

Lashkarbolooki, M., Ayatollahi, S., & Riazi, M. (2014). Effect of salinity, resin, and asphaltene on the surface properties of acidic crude oil/smart water/rock system. *Energy and Fuels*, *28*, 6820–6829. https://doi.org/10.1021/ef5015692

Leal, A. M., Blunt, M. J., & LaForce, T. C. (2013). A robust and efficient numerical method for multiphase equilibrium calculations: Application to co2-brine-rock systems at high temperatures, pressures and salinities. *Advances in Water Resources*, *62*, 409–430. https://doi.org/10.1016/j.advwatres.2013.02.006

Leal, A. M., Blunt, M. J., & LaForce, T. C. (2014). Efficient chemical equilibrium calculations for geochemical speciation and reactive transport modelling. *Geochimica et Cosmochimica Acta*, *131*, 301–322. https://doi.org/10.1016/j.gca.2014.01.038

Leal, A. M., Kulik, D. A., Kosakowski, G., & Saar, M. O. (2016). Computational methods for reactive transport modeling: An extended law of mass-action, xlma, method for multiphase equilibrium calculations. *Advances in Water Resources*, *96*, 405–422. https://doi.org/10.1016/j.advwatres.2016.08.008

Leal, A. (2015). Reaktoro: An open-source unified framework for modeling chemically reactive systems. https://reaktoro.org

Ligthelm, D. J., Gronsveld, J., Hofman, J. P., Brussee, N. J., Marcelis, F., & Linde, H. A. V. D. (2009). Spe 119835 novel waterflooding strategy by manipulation of injection brine composition. *EUROPEC/EAGE Annual Conference and Exhibition*, 1–22. https://doi.org/10.2118/119835-ms

Mahani, H., Menezes, R., Berg, S., Fadili, A., Nasralla, R., Voskov, D., & Joekar-Niasar, V. (2017). Insights into the impact of temperature on the wettability alteration by low salinity in carbonate rocks. *Energy and Fuels*, *31*, 7839–7853. https://doi.org/10.1021/acs.energyfuels.7b00776

Mahani, H., Keya, A. L., & Berg, S. (2015). Driving mechanism of low salinity flooding in carbonate rocks. *EUROPEC 2015*, 1–27. https://doi.org/10.2118/174300-ms

Mahani, H., Keya, A. L., Berg, S., & Nasralla, R. (2016). Electrokinetics of carbonate/brine interface in low-salinity waterflooding: Effect of brine salinity, composition, rock type, and ph on ζ-potential and a surface-complexation model. *SPE Journal*, (SPE-181745-PA). https://doi.org/10.2118/181745-PA

McPhee, C., Reed, J., & Zubizarreta, I. (2015). *Core analysis: A best practice guide* (1st ed., Vol. 64). Elsevier. https://libgen.li/file.php?md5=513076061bde8382b139a03579067d18

McWhorter, D. B., & Sunada, D. K. (1990). Exact integral solutions for two-phase flow. *Water Resources Research*, *26*(3), 399–413. https://doi.org/10.1029/89WR02974

Morse, J. W., Arvidson, R. S., & Morse, J. W. (2002). The dissolution kinetics of major sedimentary carbonate minerals. *Earth-Science Reviews*, *58*, 51–84. https://doi.org/10.1016/s0012-8252(01)00083-6

Mwangi, P., Brady, P. V., Radonjic, M., & Thyne, G. (2018). The effect of organic acids on wettability of sandstone and carbonate rocks. *Journal of Petroleum Science and Engineering*, *165*, 428–435. https://doi.org/10.1016/j.petrol.2018.01.033

Olivares-Xometl, O., Arellanes-Lozada, P., Lijanova, I. V., Azotla-Cruz, L., & Likhanova, N. V. (2024). Preformed oil-in-water macroemulsions for oil recovery

[Article ID: IE24252]. *Revista Mexicana de Ingeniería Química*, *23*(3), IE24252. https://doi.org/10.24275/rmiq/IE24252

Omekeh, A., Friis, A., Fjelde, I., & Evje, S. (2012). Modeling of ion-exchange and solubility in low salinity water flooding. *SPE Improved Oil Recovery Symposium*, 1–13. https://doi.org/10.2118/154144-ms

Ouden, L. (2014). *Calcite dissolution behaviour during low salinity water flooding in carbonate rock* [Master's thesis, Delft University of Technology].

Parkhurst, D. L., & Appelo, C. A. J. (2013). PHREEQC version 3. https://www.usgs.gov/software/phreeqc-version-3

Qiao, C., Li, L., Johns, R. T., & Xu, J. (2015). A mechanistic model for wettability alteration by chemically tuned waterflooding in carbonate reservoirs. *SPE Journal*, *20*, 767–783. https://doi.org/10.2118/170966-PA

Qiao, C., Li, L., Johns, R. T., & Xu, J. (2016). Compositional modeling of dissolution-induced injectivity alteration during co2 flooding in carbonate reservoirs. *SPE Journal*, *21*, 809–826. https://doi.org/10.2118/170930-pa

Qiao, C., Johns, R., & Li, L. (2016). Modeling low-salinity waterflooding in chalk and limestone reservoirs. *Energy and Fuels*, *30*, 884–895. https://doi.org/10.1021/acs.energyfuels.5b02456

Rahevar, S., Kakati, A., Kumar, G., Sangwai, J., Myers, M., & Al-Yaseri, A. (2023). Controlled salinity water flooding and zeta potential: Insight into a novel enhanced oil recovery mechanism. *Energy Reports*, *9*, 2557–2565. https://doi.org/10.1016/j.egyr.2023.01.088

Reinoso, B. S., Mohanty, K. K., & Panda, M. (2024). Synergistic impact of low salinity and surfactant on wettability alteration in carbonates. *SPE Symposium on Improved Oil Recovery*, *2024-April*. https://doi.org/10.2118/218196-MS

Sakuma, H., Andersson, M., Bechgaard, K., & Stipp, S. (2014). Surface tension alteration on calcite, induced by ion substitution. *The Journal of Physical Chemistry C*, *118*, 3078–3087. https://doi.org/10.1021/jp411151u

Sanaei, A., Tavassoli, S., & Sepehrmoori, K. (2019). Investigation of modified water chemistry for improved oil recovery: Application of DLVO theory and surface complexation model. *Colloids and Surfaces A: Physicochemical and Engineering Aspects*, *574*, 131–145. https://doi.org/10.1016/j.colsurfa.2019.04.075

Serrano-Saldaña, E. (2018). *Resultados de pruebas de imbibición espontánea en muestras de caliza* (Technical Report No. D.61057). Instituto Mexicano del Petroleo.

Tanger, J. C., & Helgeson, H. C. (1988). Calculation of the thermodynamic and transport properties of aqueous species at high pressures and temperatures; revised equations of state for the standard partial molal properties of ions and electrolytes. *American Journal of Science*, *288*(1), 19–98. https://doi.org/10.2475/ajs.288.1.19

Tetteh, J. T., & Barati, R. (2019). Crude-oil/brine interaction as a recovery mechanism for low-salinity waterflooding of carbonate reservoirs. *SPE Reservoir Evaluation and Engineering*, *22*, 877–896. https://doi.org/10.2118/194006-PA

Tetteh, J. T., Brady, P. V., & Ghahfarokhi, R. B. (2021). Impact of temperature and so42- on electrostatic controls over carbonate wettability. *Colloids and Surfaces A: Physicochemical and Engineering Aspects*, *625*, 1–32. https://doi.org/10.1016/j.colsurfa.2021.126893

Wei, B., Lu, L., Li, Q., Li, H., & Ning, X. (2017). Mechanistic study of oil/brine/solid interfacial behaviors during low-salinity water flooding using visual and quantitative methods. *Energy Fuels*, *31*, 6615–6624. https://doi.org/10.1021/acs.energyfuels.7b00825

Xie, Q., Brady, P. V., Pooryousefy, E., Zhou, D., Liu, Y., & Saeedi, A. (2017). The low salinity effect at high temperatures. *Fuel*, *200*, 419–426. https://doi.org/10.1016/j.fuel.2017.03.088

Xie, Q., Sari, A., Pu, W., Chen, Y., Brady, P. V., Maskari, N. A., & Saeedi, A. (2018). Ph effect on wettability of oil/brine/carbonate system: Implications for low salinity water flooding. *Journal of Petroleum Science and Engineering*, *168*, 419–425. https://doi.org/10.1016/j.petrol.2018.05.015

Yousef, A. A., Al-Saleh, S., Al-Kaabi, A., & Al-Jawfi, M. (2011). Laboratory investigation of the impact of injection-water salinity and ionic content on oil recovery from carbonate reservoirs. *SPE Reservoir Evaluation and Engineering*, *14*, 578–593. https://doi.org/10.2118/137634-PA

Yu, L., Evje, S., Kleppe, H., Kårstad, T., Fjelde, I., & Skjaeveland, S. M. (2009). Spontaneous imbibition of seawater into preferentially oil-wet chalk cores - experiments and

simulations. *Journal of Petroleum Science and Engineering*, *66*, 171–179. https://doi.org/10.1016/j.petrol.2009.02.008

Zaeri, M. R., Hashemi, R., Shahverdi, H., & Sadeghi, M. (2018). Enhanced oil recovery from carbonate reservoirs by spontaneous imbibition of low salinity water. *Petroleum Science*, *15*, 564–576. https://doi.org/10.1007/s12182-018-0234-1

Zhang, P., Tweheyo, M. T., & Austad, T. (2007). Wettability alteration and improved oil recovery by spontaneous imbibition of seawater into chalk: Impact of the potential determining ions ca2+, mg2+, and so42-. *Colloids and Surfaces A: Physicochemical and Engineering Aspects*, *301*, 199–208. https://doi.org/10.1016/j.colsurfa.2006.12.058